NASA
SPACE VEHICLE
DESIGN CRITERIA
(STRUCTURES)

NASA SP-8040

FRACTURE CONTROL OF METALLIC PRESSURE VESSELS

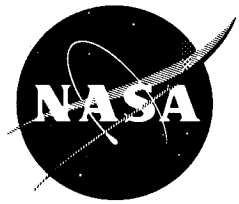

MAY 1970

NATIONAL AERONAUTICS AND SPACE ADMINISTRATION

FOREWORD

NASA experience has indicated a need for uniform criteria for the design of space vehicles. Accordingly, criteria are being developed in the following areas of technology:

Environment
Structures
Guidance and Control
Chemical Propulsion

Individual components of this work will be issued as separate monographs as soon as they are completed. A list of all previously issued monographs in this series can be found at the end of this document.

These monographs are to be regarded as guides to design and not as NASA requirements, except as may be specified in formal project specifications. It is expected, however, that the criteria sections of these documents, revised as experience may indicate to be desirable, eventually will become uniform design requirements for NASA space vehicles.

This monograph was prepared under the cognizance of the Langley Research Center. The Task Manager was W. C. Thornton. The author was C. F. Tiffany of The Boeing Company. A number of other individuals assisted in developing the material and reviewing the drafts. In particular, the significant contributions made by C. P. Berry and R. A. Rawe of McDonnell Douglas Corporation; D. W. Hoeppner of Lockheed-California Company; R. L. Johnston of NASA Manned Spacecraft Center; G. F. Kappelt of Bell Aerosystems Company; J. M. Krafft of the U. S. Naval Research Laboratory; G. T. Smith of Lewis Research Center; H. G. McComb, Jr., of Langley of Grumman Aircraft Engineering Corporation; J. C. Lewis of Jet Propulsion Laboratory; G. T. Smith of Lewis Research Center; H. G. McComb, Jr. of Langley Research Center; and C. D. Crockett of NASA George C. Marshall Space Flight Center are hereby acknowledged.

May 1970

For sale by the National Technical Information Service, Springfield, Virginia 22151 — Price $3.00

CONTENTS

FRACTURE CONTROL OF METALLIC PRESSURE VESSELS

1. INTRODUCTION

Pressure vessels often contain small flaws or defects that are inherent in the materials or introduced during a fabrication process. These defects can, in many cases, cause severe reduction in the load-carrying capability and the operational life of pressure vessels. If the flaws are large in comparison to those causing failure at the proof-pressure stress levels, failure of the vessels will occur during initial pressurization. If the initial flaws are small, the vessels may withstand several operational pressure cycles and a number of hours of sustained-pressure loading before the flaws grow to a size that will result in failure. From an economic standpoint, it is important to minimize the possibility of failure of space vehicle pressure vessels during proof testing. From the standpoint of economics and personnel safety, it is imperative to prevent mission or operational failures.

During the past several years there have been costly proof-test failures directly attributable to small, preexisting flaws. In one example, a large steel rocket motor case failed at a stress less than 50 percent of the material yield strength. This failure originated at a small internal flaw having a depth less than one fifth of the material thickness. Other proof-test failures occurred in large propellant tanks and smaller auxiliary tanks used in the Apollo program.

Other failures have occurred after proof testing during the preflight checkout and/or storage of pressure vessels. One such failure occurred when a high-pressure helium tank, used in a defensive missile system, ruptured after 21 hours of sustained pressurization. This failure originated at an inclusion in the parent metal. The initial flaw increased approximately 50 percent in size during the time the tank was pressurized, and failure resulted. Although this is an example of failure resulting from flaw growth under sustained stress in a relatively inert environment, many more failures have occurred in which the environment played the dominant role. A number of titanium pressure vessels failed in N_2O_4 and methanol environments, and high-strength steel vessels failed in water environments. In these cases, the initial flaw sizes were often small (i.e., less than 10 percent of the size required to cause failure) and could not have been detected by nondestructive inspection. However, with the vessels at pressure for a time, the

environment induced significant amounts of stable flaw growth and the vessels eventually failed.

The purpose of this monograph is to present criteria and recommend practices that aid in the design of metallic pressure vessels by minimizing the occurrence of proof-test failures resulting from cracks and assuring against preflight and flight failures. The criteria and recommended practices permit wide latitude in the selection of materials and operational stress levels, detail design, analysis, and test to allow minimization of weight and/or cost as may be dictated by specific vehicle and mission requirements. This monograph is applicable to metallic pressure vessels whose design is primarily controlled by internal pressure requirements. These vessels include high-pressure gas bottles, solid-propellant motor cases, and storable and cryogenic liquid-propellant tanks – both integral and removable. Criteria and recommended practices for the design of pressurized cabins, inflatable structures, and vessels fabricated from composite materials will be presented in other monographs planned for this series.

To minimize proof test and prevent service failures of metallic pressure vessels, the three basic considerations are (1) the initial flaw sizes, (2) the critical flaw sizes (i.e., the sizes required to cause fracture at a given stress level), and (3) the subcritical flaw-growth characteristics. To prevent proof-test failures, the actual initial flaw sizes must be less than the critical flaw sizes at the proof-stress level. To guarantee that the vessel will not fail in service, it must be shown that the largest possible initial flaw in the vessel cannot grow to critical size during the required life span of the vessel. The basic parameters affecting critical flaw sizes are the applied stress levels, the material fracture toughness values, the pressure-vessel wall thickness, and the location and orientation of flaws. The determination of actual initial flaw sizes is limited by the capabilities of the available nondestructive inspection procedures; however, this limitation can often be partially circumvented by using information obtained from a successful proof test. A proof test in which the vessel does not fail provides information on the maximum possible initial-to-critical stress-intensity ratio within the vessel which, in turn, allows the size of the maximum possible initial flaw to be estimated. Subcritical flaw growth depends on several factors including the stress level, initial flaw size, environment, material, and pressure/time history of the particular pressure vessel.

Because many factors are involved, it is unlikely that the problem of premature fracture of pressure vessels will be completely resolved in the immediate future. During the past 10 to 15 years, however, significant progress has been made in several different areas (i.e., mechanics, metallurgy, inspection, etc.); accomplishments in the field of fracture mechanics have been particularly significant. Linear-elastic fracture mechanics has provided a basic framework and engineering language for describing the fracture of materials under static, cyclic, and sustained-stress loading, and is the basis for the criteria and recommended practices presented in this monograph.

The related problems of stress corrosion, fatigue, and discontinuities in pressure-vessel design will not be treated herein, but will be covered in other monographs now in preparation.

2. STATE OF THE ART

The problem of premature fracture of metallic structures is not new (e.g., the large molasses tank failure in 1919, the methane storage tank failure in 1944, the 25-percent failure rate of Liberty ships during World War II, and the Polaris motor case failures during the 1950's). Even today there is a general lack of specific guides in industry and government manuals, specifications, and codes for the control of fracture of metallic pressure vessels. This results from the complexity and interdisciplinary nature of the problem, the lengthy time required to develop and verify experimentally the technical approaches, and the differing opinions on technical approach. The design of metallic pressure vessels generally has been (and to some extent, is still) based on the following principles:

1. The gross stress levels at the proof and operating conditions should be kept below the yield strength of the material to prevent large-scale deformations.

2. The fracture strength will be greater than the yield strength and equal to or greater than the minimum guaranteed ultimate tensile strength of the material.

3. Local yielding may occur around discontinuities, but the overall structural integrity will be maintained by load relief and redistribution.

4. The factor of safety provides for uncertainties in stress analysis, fabrication, and applied loads, and allows for possible degradation in strength with service life.

5. Selection of factors of safety should be based primarily on experience, a qualitative assessment of the uncertainties associated with a specific design, and the reliability requirements.

6. Sharp-edged flaws or defects will not be allowed and, if any occur, they will be detected by nondestructive inspection and subsequently repaired.

Although many apparently successful pressure vessels have been designed according to the above principles, there have been many costly failures at gross stress levels well below the yield strength. In many of these cases, local yielding did not occur, sharp-edged flaws were missed by inspection, and the past experiences used in selection of the factors of safety were not applicable.

Various approaches have been suggested for use in the control of premature fracture. In reference 1, E. T. Wessel and his coworkers compare and appraise a number of these approaches, primarily on the basis of their applicability to engineering design and material evaluation. They classify the approaches into the two general categories of transition temperature and stress analysis. The lack of an abrupt ductile-to-brittle transition in high-strength steel, aluminum, and titanium alloys combined with a lack of quantitativeness eliminated the transition temperature approaches from consideration. The various stress analysis approaches, based on either stress or strain criteria of fracture, had not been developed sufficiently, lacked quantitativeness, or could not handle the fracture control problem with the desired degree of completeness. It was concluded from this study that linear-elastic fracture mechanics was the approach best suited to design application. The same conclusion was reached by other investigators, both before and after the study.

The primary limitation of linear-elastic fracture mechanics to date is that at stress levels above the yield strength of the material, fracture cannot be described by the critical stress-intensity parameter, K_{Ic}, and subcritical flaw growth cannot be described as a function of the crack-tip stress-intensity factor, K_I. From the standpoint of application, this means that at stress levels above the yield strength, critical flaw size and subcritical flaw-growth data must be obtained empirically over a range of flaw sizes for the specific material and thickness of interest. Also, from the standpoint of fracture testing, it means that extremely thick test specimens are required to cause fracture prior to general yielding and thus obtain K_{Ic} values for materials with a high fracture resistance (refs. 2 and 3). Another limitation is the relatively small quantity of fracture toughness and subcritical flaw-growth data that is generally available.

A less important limitation of fracture mechanics is that stress-intensity solutions, to describe accurately the functional relationship between flaw size and stress level for various flaw shapes and boundary stress conditions, are still under development. Upon completion, these solutions should improve the accuracy of critical flaw-size estimates and pressure-vessel life predictions. However, at the present state of development, fracture specimen test data and fracture mechanics analysis can be used to predict critical flaw sizes and failure modes, to estimate minimum structural life, to establish proof-test factors and proof-testing procedures, to provide a basis for establishing nondestructive inspection flaw acceptance limits, to compare candidate materials, to assist in basic alloy development, to perform failure analyses, and finally (and perhaps

most importantly), to provide a framework for understanding the interrelationships between the various factors that affect the flightworthiness and weight of metallic pressure vessels.

2.1 Critical Flaw Sizes

Flaw types that often go undetected in metallic pressure vessels are the surface and embedded flaws. The flaw size required to cause fracture at a given applied stress level is called the critical size. If the vessel contains an initial flaw which exceeds the critical size at the proof-stress level, catastrophic failure can be expected during proof testing. Failure during service operation will occur when the initial flaw is less than the critical size at the proof-stress level, but grows with service usage until it reaches the critical size at the operating stress level. Pressure vessel leakage occurs when an initial flaw grows through the thickness of the vessel wall prior to reaching critical size.

In elastic stress fields, the critical sizes for surface and internal flaws depend on the plane-strain critical stress-intensity or fracture toughness values (K_{Ic}) of the vessel materials, and the applied stress levels. If the critical flaw sizes are small with respect to the wall thickness of the pressure vessel, the vessel is termed "thick walled." If the critical sizes approach or exceed the wall thickness, the vessel is termed "thin walled."

The critical flaw sizes for surface flaws in uniformly stressed thick-walled vessels can be calculated using the following expression:

$$(a/Q)_{cr} = \frac{1}{1.21\pi}\left(\frac{K_{Ic}}{\sigma}\right)^2 \qquad (1)$$

For small internal flaws the same expression can be used except the 1.21 coefficient is decreased to unity.

Figure 1 shows the relationship between the flaw-shape parameter, Q, and the flaw depth-to-length ratio; figure 2 is a graphical representation of equation (1).

To predict critical flaw sizes (as well as failure modes and operational life) of thin-walled pressure vessels, it is necessary to know the stress intensity for flaws that become very deep with respect to the wall thickness. The stress-intensity solution shown in equation (1) for the semielliptical surface flaw was derived by Irwin (ref. 4) and was found to be reasonably accurate for flaw depths up to about 50 percent of the material thickness. At greater depths, the applied stress intensity is magnified by the effect of the free surface near the flaw tip. This means that in thin-walled vessels, the flaw-tip stress intensity can attain the critical value (i.e., the K_{Ic} value) at a flaw size significantly smaller than that which would be predicted using equation (1).

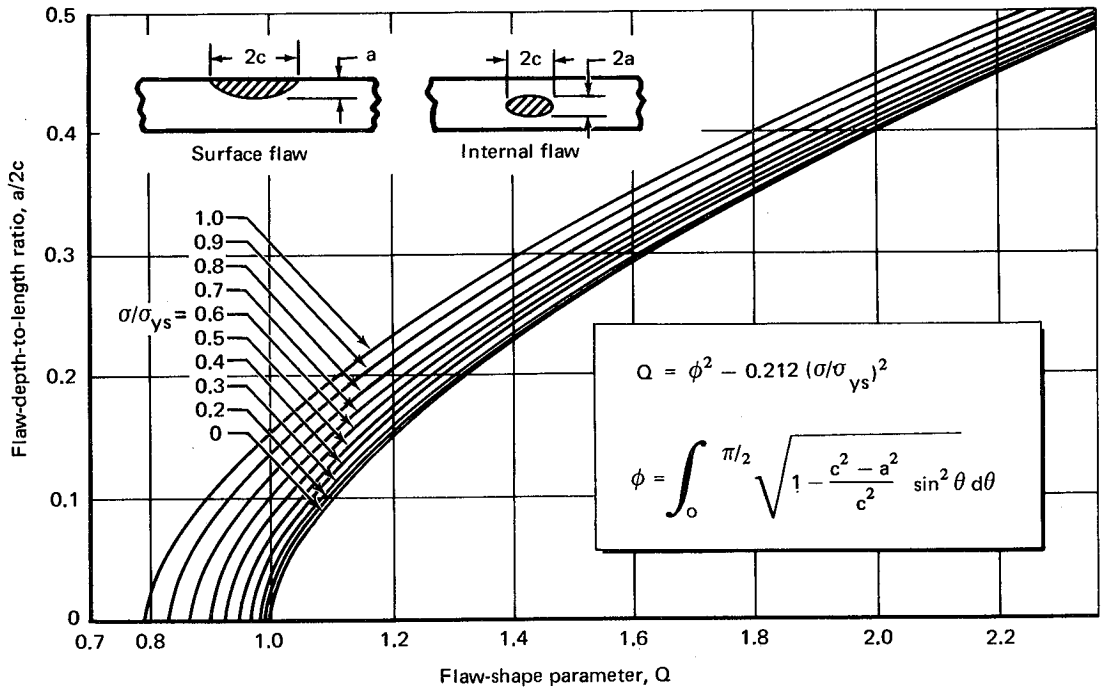

Figure 1 – Flaw-shape parameter curves

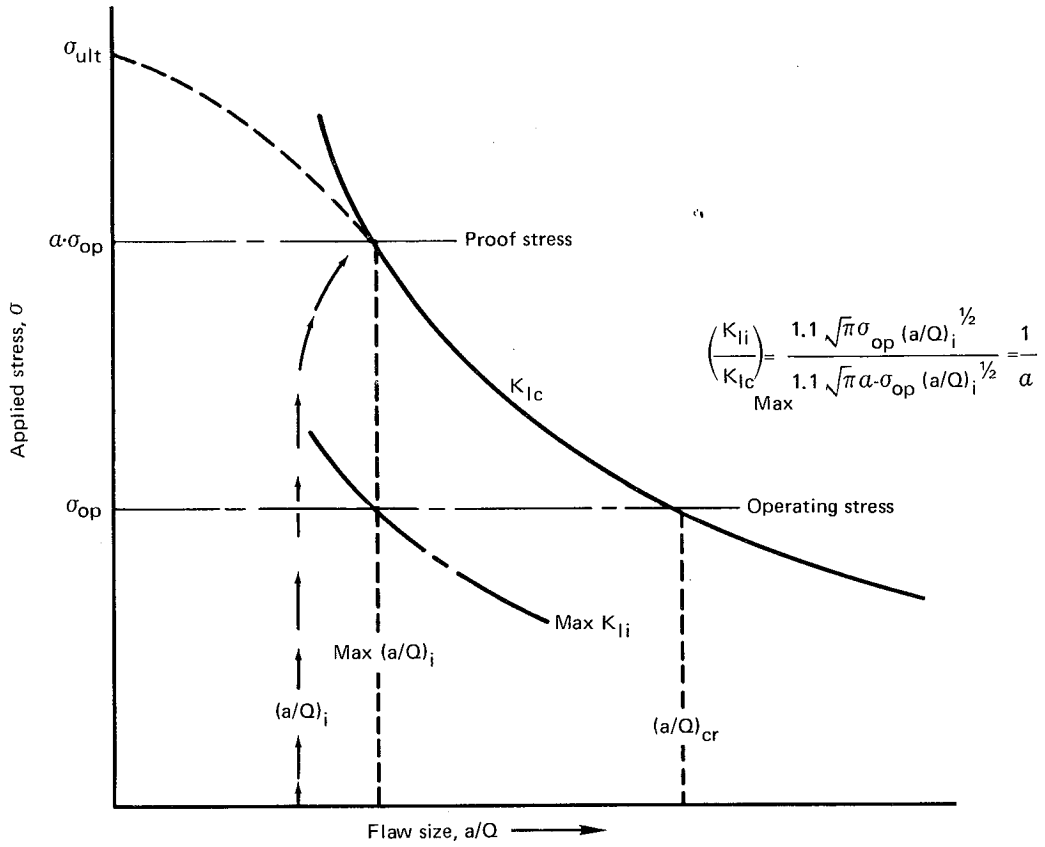

Figure 2. – Applied stress vs critical flaw size.

Kobayashi and Smith developed approximate solutions for deep surface flaws that are very long with respect to their depth (i.e., small a/2c values) and for semicircular surface flaws (i.e., a/2c = 0.5), respectively (refs. 5 and 6). Results of their solutions are shown in terms of a stress-intensity magnification factor, M_K, versus a/t in figure 3. Reference 7 shows an estimate made by NASA/MSC of how M_K varies as a function of a/2c between values of a/2c of 0 and 0.5. The M_K factor is applied to the original Irwin equation to obtain the stress intensity for deep surface flaws. The magnification reaches a maximum value of less than 10 percent for semicircular flaws, whereas there is an increase of about 60 percent for flaws having smaller values of a/2c.

Experimental data obtained on several materials with varying flaw sizes and flaw shapes appear to provide a fair degree of substantiation of the available approximate solutions (ref. 8). An exact numerical solution for deep, semielliptical, surface flaws with varying values of a/2c is under development, and additional experimental investigations are being performed.

To illustrate the effect of the deep-flaw stress-intensity magnification on predicted critical flaw sizes, it is convenient to assume that the vessel contains flaws which are long with respect to their depth. When the flaw-shape parameter, Q, is approximately equal to unity (i.e., for long flaws), the flaw size can be described in terms of the flaw depth, a. A predicted critical flaw-size curve (obtained using Kobayashi's M_K curve) for

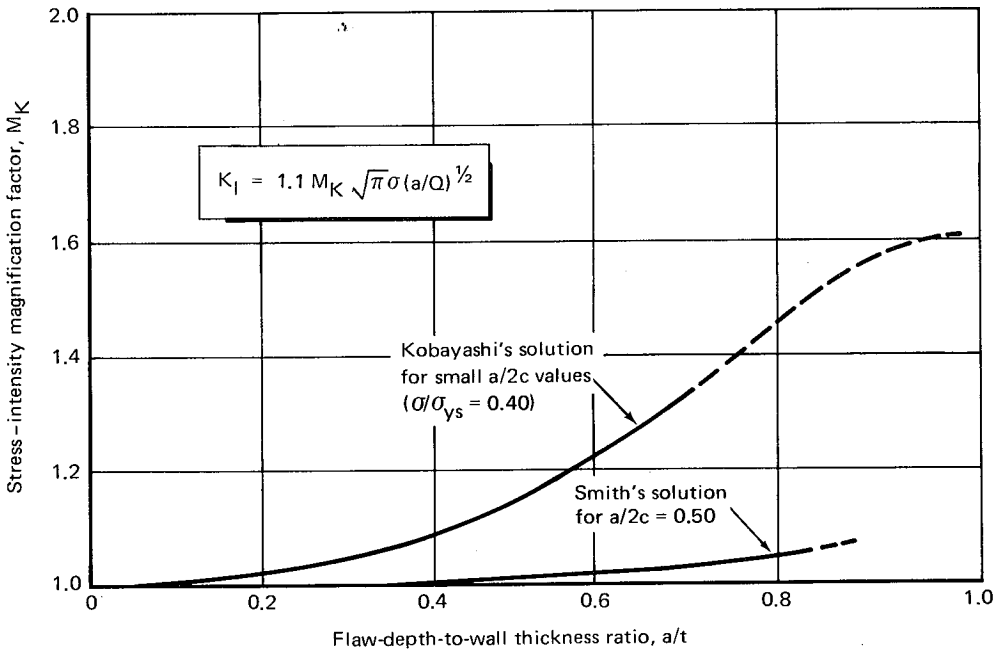

Figure 3. – Stress-intensity magnification factors for deep surface flaws.

a typical tank material and wall thickness is shown in figure 4. Also shown for comparison is the critical flaw-size curve for the same material in a thick-walled vessel. The curve for the thin-walled vessel is characterized by a significant reduction in failing stress at a given flaw size as compared to that for the thick-walled vessel. The life and potential failure modes of these thin-walled vessels are schematically illustrated in figure 5. The failure mode for thin-walled vessels can be complete fracture if the critical flaw depth is less than the wall thickness at the operating stress level (figure 5A). Figure 5B illustrates the case where the critical flaw depth is greater than the wall thickness at the operating stress level and the resulting failure mode is leakage.

From equation (1) it is apparent that to predict the critical sizes for surface and internal flaws it is necessary to know the plane-strain fracture toughness (K_{Ic}) values for the vessel materials (i.e., parent metal, welds, etc.). In heavy-gage, high-strength materials or in thin-gage materials that are relatively brittle, it is generally a straightforward task to obtain K_{Ic} values from laboratory tests. Several types of test specimens are used to measure K_{Ic}values. These include fatigue-cracked bend specimens, surface-flawed specimens, crack-line loaded specimens, center-cracked and edge-cracked sheet specimens, and fatigue-cracked round notched-bar specimens. Testing requirements, limitations, advantages, and disadvantages of these various types of test specimens are discussed in considerable detail in references 2 and 3.

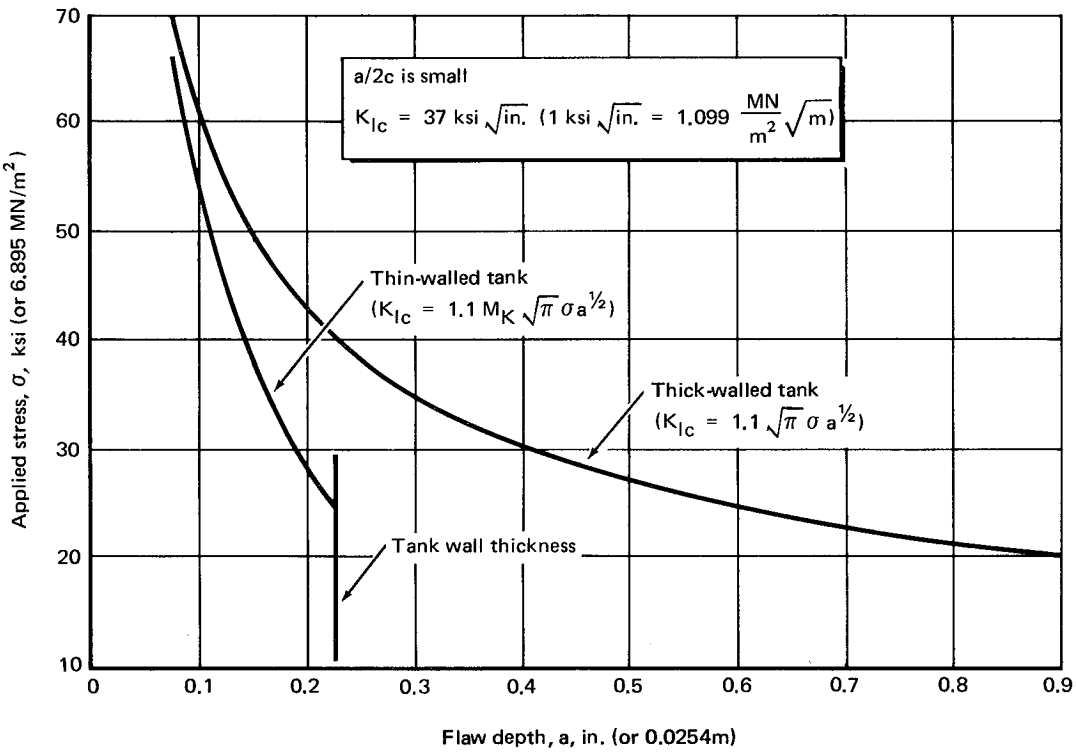

Figure 4. – Critical flaw-size curves at LO_2 temperature for 2219-T87 aluminum

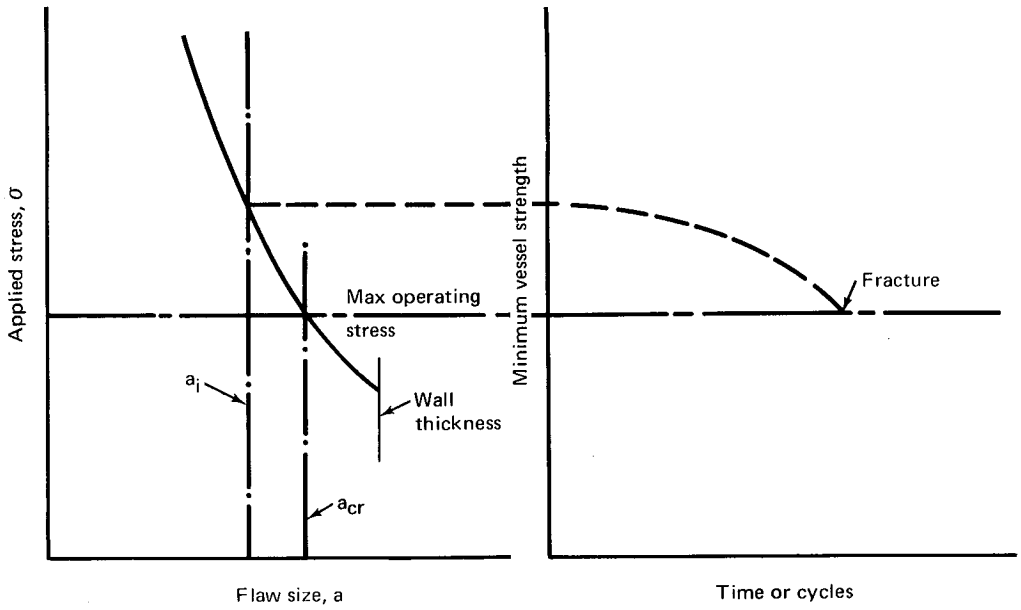

A. Failure mode = fracture

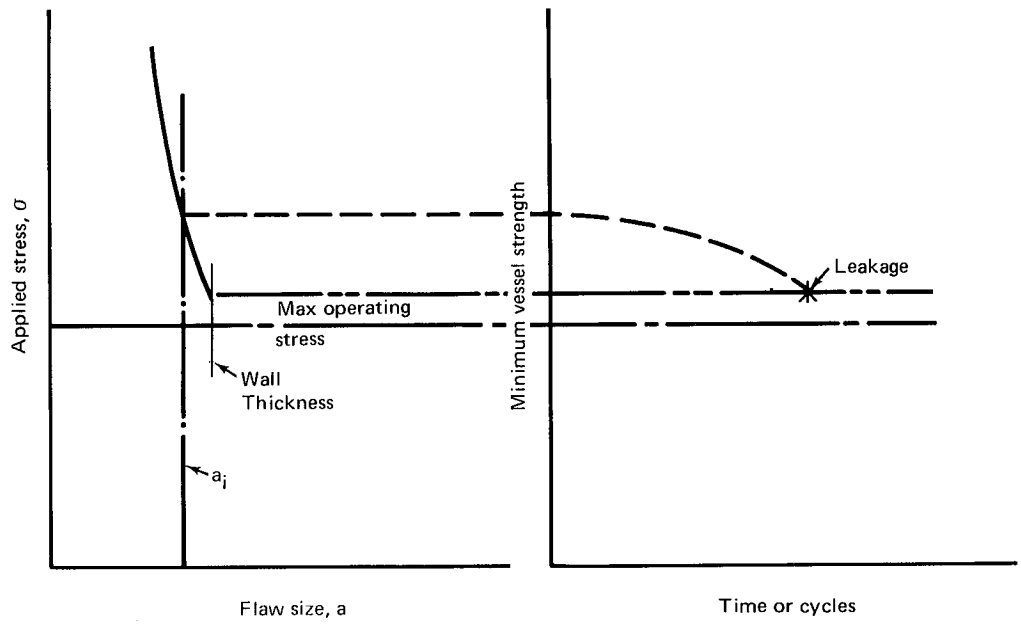

B. Failure mode = leakage

Figure 5. – Schematic representation of thin-walled vessel life.

For predicting critical flaw sizes in aerospace pressure vessels, the surface-flawed specimen has probably been the most widely used. However, the fatigue-cracked bend specimen has the distinct advantage of being the only test specimen for which a detailed proposed recommended practice has been published by the American Society for Testing Materials (ref. 9).

In thin-gaged materials with moderate-to-high toughness, as well as all other situations where the fracture stress levels exceed the yield strength, it is necessary to obtain critical flaw-size data empirically. This was generally accomplished by testing a series of surface-flawed specimens with thickness equal to the pressure-vessel wall thickness and having various initial flaw sizes. Examples of such specimen tests are included in references 10 and 11. Also, an example of such test data is shown in figure 6. These data were obtained from reference 12.

2.2 Initial Flaw Size

To prevent failure, either the actual initial flaw sizes or the maximum possible initial flaw sizes (or initial stress-intensity factors) of pressure vessels must be known. Nondestructive inspection is the only means of determining actual initial flaw sizes. A successful proof test can provide a measure of the maximum possible initial-to-critical stress-intensity ratio, and in turn allows the maximum possible initial flaw size to be estimated.

2.2.1 Nondestructive Inspection

The more common inspection techniques for inspection of aerospace pressure vessels are radiographic, ultrasonic, penetrant, and magnetic particle. Other techniques investigated for potential production usage include eddy current and infrared (ref. 13). Several studies have been performed during the past several years to evaluate the capabilities of these various techniques to detect the different types of flaws found in pressure vessels (refs. 13 and 14). Results of these studies, combined with actual pressure-vessel inspection experience, lead to the following general conclusions:

1. With the use of multiple inspection systems (e.g., X-ray, ultrasound, and penetrant), most surface and internal flaws encountered in pressure vessels can be, and generally are, detected. However, it is unsafe to assume that all potentially dangerous flaws will be found at all times (e.g., tight cracks are particularly difficult to detect).

2. The lower limits of inspection detection capability (i.e., the largest initial flaw sizes which can escape detection) cannot be confidently established.

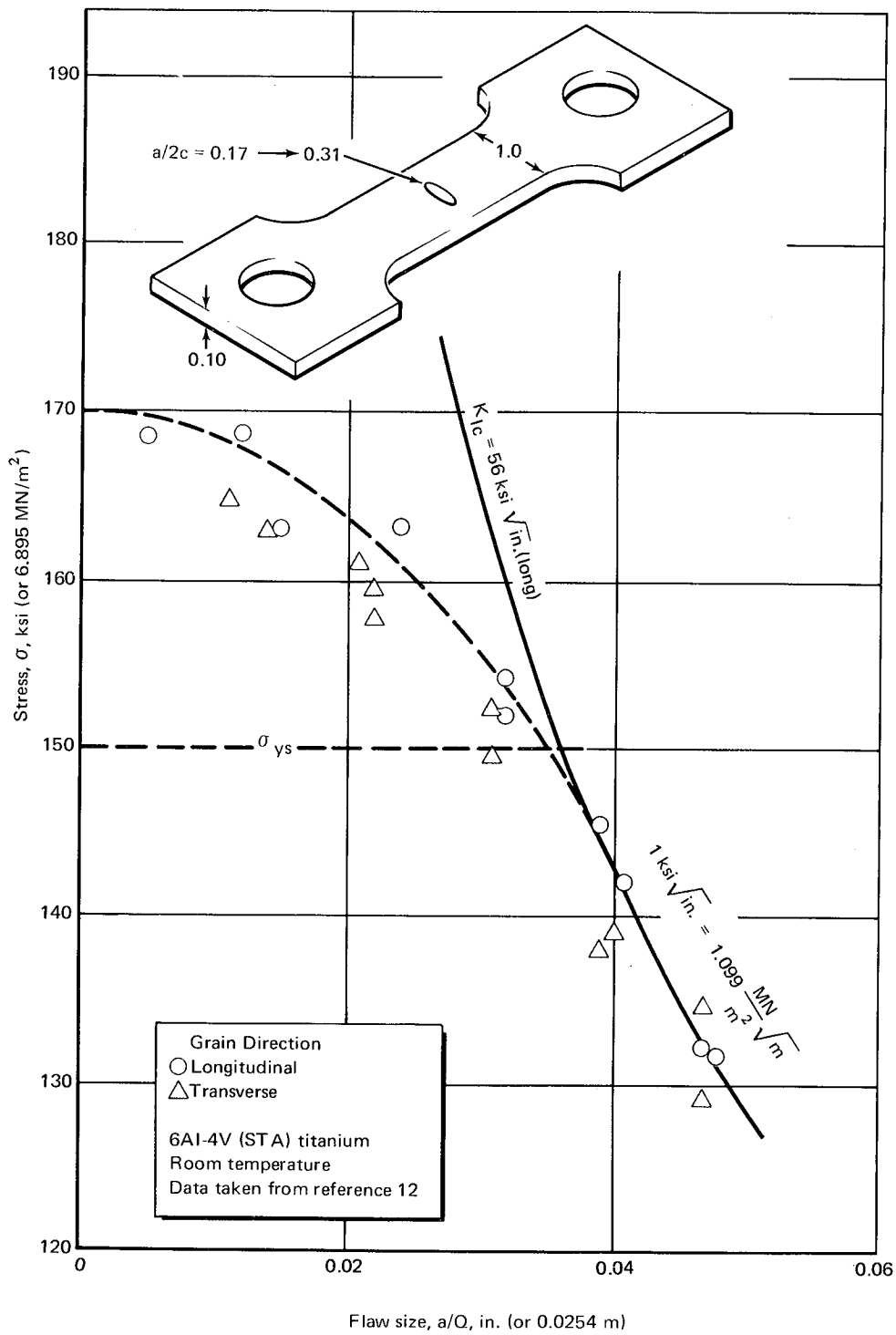

Figure 6. – Empirical critical flaw size data

3. The inspection procedures commonly used do not provide the precise measure of initial flaw sizes (i.e., length and depth) necessary for use in a fracture mechanics analysis.

4. Regardless of the limitations of the techniques, there is no practical alternative but to rely on nondestructive inspection to prevent proof-test failures of most high-strength pressure vessels.

2.2.2 Proof Test

For many years, it was normal practice to perform proof-pressure tests on pressure vessels; these tests, in effect, have served at least as one of the final inspections prior to service usage of the vessels. However, prior to about 1960, very little was understood regarding the determination of proof-test factors and proof-test procedures to minimize potential damaging effects of the test, yet ensure adequate subsequent service performance. During the past ten years, it has become apparent from the results of fracture mechanics studies and aerospace pressure-vessel experience that a properly designed and successfully executed proof-pressure test is probably the most reliable nondestructive inspection technique available for insuring that there are no initial flaws of sufficient size to cause failure under operating conditions.

It was originally pointed out in reference 15 and illustrated in figure 2 of this document, that a successful proof test to a pressure of a times the maximum operating pressure indicates that the maximum possible K_{Ii}/K_{Ic} at the maximum operating pressure is equal to $1/a$ and that this value could be used with subcritical flaw-growth data to estimate the minimum life of the pressure vessel. Additionally, it is generally true that the validity of the minimum life predictions do not depend upon accurate values of either the actual applied stress levels or the fracture toughness (K_{Ic}), both of which vary throughout a given vessel. However, it should be noted that to estimate the maximum possible initial flaw sizes in any specific area of the vessel, it is necessary to know the accurate applied stress levels and the K_{Ic} values.

From the standpoint of initial design, the minimum required proof-test factor for a pressure vessel is $a = 1 \div$ allowable K_{Ii}/K_{Ic}. The allowable value of K_{Ii}/K_{Ic} depends on the required service life of the vessel and the subcritical flaw-growth characteristics of the vessel materials and, ideally, should be a statistically meaningful value obtained from laboratory test data.

Since the introduction of the proof-test concept, based on fracture mechanics, concern has been expressed about possible damaging effects of the proof test; there has been speculation that the test could cause the operational failure of a vessel that might have

performed satisfactorily had a proof test not been performed. Subcritical flaw growth can, and often does, occur in relatively inert environments. Therefore, it is likely that during the time required to perform a proof test, initial flaws or defects in the vessel that are evident can increase in size or possibly flaws which were not evident could be opened up. In fact, if the proof test is not properly designed (e.g., if a is $< 1 \div$ allowable K_{Ii}/K_{Ic}, depressurization rates are too slow, or the test is conducted with an aggressive test fluid), the flaw growth occurring during the test could be sufficient to cause an operational failure.

During the past several years there have been numerous questions about the value of the proof test with regard to the effects of applied stress levels and pressure-vessel wall thickness, selection of the test temperature, test fluids, pressurization and depressurization rates, time at maximum pressure, multiple proof-test cycles, the need for postproof inspection, and the need to simulate service loads other than internal pressure. At present, there does not appear to be unanimity of opinion throughout industry on the effects of these items. However, based on the premise that most pressure-vessel failures result from the existence and growth of flaws, several observations and analyses can and have been made. These are summarized in the following paragraphs.

2.2.2.1 Effect of Applied Stress Levels

To prevent general yielding during proof testing, pressure-vessel membrane stresses are normally limited to a value equal to or less than the yield strength of the material. However, in practice, local stress levels often exceed the yield strength as a result of design or manufacturing discontinuities and/or residual stresses. Also, in some cases (e.g., cryoformed stainless steel vessels), the entire vessel may be purposely subjected to stress levels well above the yield strength.

As shown in figure 2, when the applied stress approaches and exceeds the yield strength of the material, the critical flaw-size curve deviates from the theoretical curve based on a constant K_{Ic} so that critical flaw sizes are smaller than those predicted by linear-elastic fracture mechanics. If the applied stresses in a pressure vessel at proof pressure exceed the yield strength, and if the vessel passes the proof test, the maximum possible K_{Ii}/K_{Ic} proven by the test is smaller than $1/a$. The minimum operational life of the vessel then should exceed the required life, which was used to determine a originally. A potentially beneficial effect of high proof-stress levels is that flaws may tend to be blunted and, as a result, the subcritical flaw growth during operational use of the vessel could be retarded. An apparent disadvantage is that at high proof-stress levels the critical flaw sizes may be very small compared to those that can normally be detected; thus the proof-test failure rate may be quite high.

2.2.2.2 Effect of Wall Thickness

It has been shown by analysis that regardless of the pressure-vessel wall thickness, the required minimum proof-test factor a is 1 ÷ allowable K_{Ii}/K_{Ic}. However, the value of the proof test in providing assurance against service failure changes with decreasing wall thickness and/or increasing fracture toughness, K_{Ic}, the same as occurs with the predicted pressure-vessel failure mode. This is discussed in more detail in reference 16 and illustrated in figure 7.

2.2.2.3 Effect of Proof-Test Temperature

If the proof test is performed at a different temperature than service operating temperature, the required minimum proof-test factor a is as follows:

$$a = \frac{1}{\text{Allowable } K_{Ii}/K_{Ic} \text{ at operating temperature}} \times \frac{K_{Ic} \text{ at proof-test temperature}}{K_{Ic} \text{ at operating temperature}} \tag{2}$$

The advantages of testing at a temperature where the value of K_{Ic} is lower than it is at the operational temperature are as follows: (1) a lower proof-test factor can be used to guarantee the same operational life as guaranteed by the corresponding higher proof-test factor at the operational temperature, and (2) a larger operational life can be assured by using the same proof-test factor as the one at operational temperature. The disadvantage is the need to know accurately how K_{Ic} varies with temperature for all of the materials in the vessel as well as the statistical variation in K_{Ic} for each material. Also possible increased risk of proof-test failures is associated with the second case.

2.2.2.4 Effect of Test Fluids

During the late 1950's it became apparent that the test fluid was often a major factor contributing to the many proof-test failures that were being experienced. At that time considerable emphasis was placed on the use of high-strength steel alloys in solid-propellant motor cases, and it was common practice to perform the proof test using water as the test fluid. One of the first systematic studies on the detrimental effects of water on high-strength steel motor cases was performed by Shank *et al.* (ref. 17). In this study it was shown that by the mechanism of hydrogen cracking, the water was promoting slow flaw growth that eventually resulted in failure of the motor cases. With the use of oil as the proof-test fluid, the problem was overcome. Similar results were obtained by researchers in other studies.

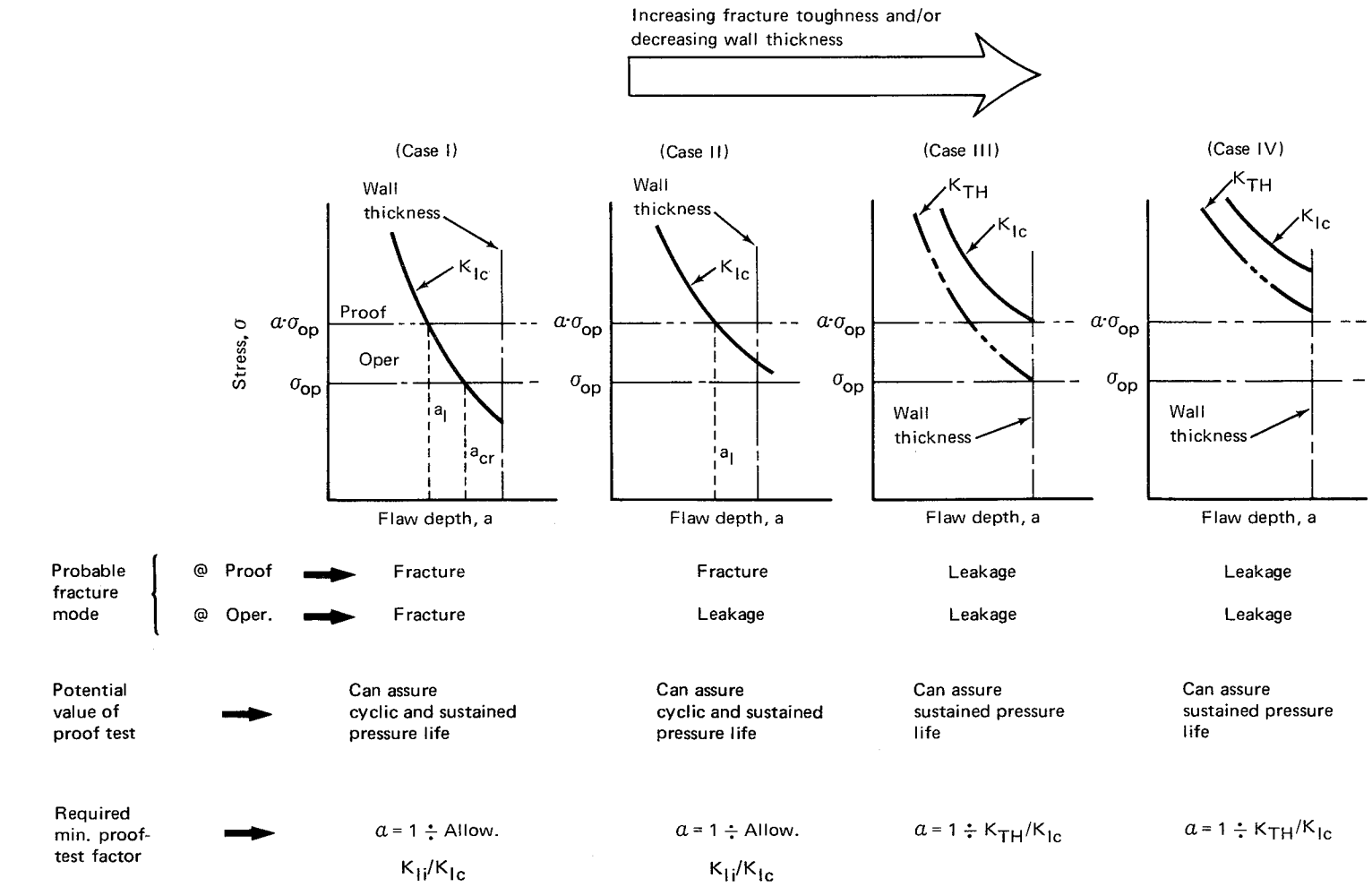

Figure 7. – The effect of wall thickness on value of proof test.

As the heat treat strength levels of steel alloys are reduced, they seem to become less and less susceptible to water-induced flaw growth [e.g., water is often used as a proof-test fluid for steel alloys having a yield strength below about 180 to 200 ksi (1 ksi = 6.895 MN/m^2)]. Corrosion inhibitors, such as sodium dichromate, are often used in the water; distilled water is sometimes used; and some pressure-vessel fabricators use demineralized water. While these measures may be quite effective in inhibiting general pitting corrosion, there appears to be little or no evidence that they will inhibit flaw growth under sustained stress if a flaw is present.

The selection of the proper proof-test fluid is an important consideration for all alloys. With precracked tensile specimens tested under sustained stress in the intended test fluid, it is possible to obtain a measure of the adequacy of the fluid for use in the proof test. (See sections 2.3 and 4.)

2.2.2.5 Effect of Test Duration and Pressurization/Depressurization Rate

If the vessel is pressurized slowly, or if the proof pressure is sustained for a long period of time, the probability of a proof-test failure is increased because of possible slow flaw growth. However, after a successful test it can still be said that the maximum possible K_{Ii}/K_{Ic} at the operating pressure is equal to $1/a$. On the other hand, if the vessel is depressurized slowly so that the flaw that was just smaller than the critical size at the proof-stress level continues to grow, the maximum possible K_{Ii}/K_{Ic} after the test will be greater than $1/a$. In fact, it appears that if the rate of increase in stress intensity caused by flaw growth is greater than the rate of decrease in stress intensity caused by reduction in stress, the vessel could even fail during depressurization.

The amount of flaw growth that will occur during depressurization depends upon the actual K_{Ii}/K_{Ic} ratio (or initial flaw size) at the start of depressurization, the depressurization rate, and the flaw-growth characteristics of the vessel materials under sustained stress in the proof-test fluid. If it is assumed that the K_{Ii}/K_{Ic} ratio approaches unity (i.e., the vessel is just about to fail) at the start of depressurization, and if sustained-stress flaw growth-rate data for the material in the test fluid are available, it is possible to determine the maximum possible K_{Ii}/K_{Ic} at the start of the vessel's operational life as a function of depressurization time. This has been done for some specific material and test fluid combinations in reference 7.

2.2.2.6 Effect of Multiple Proof Tests

In general, it appears that very little can be gained by performing multiple-cycle proof tests. Even after the last cycle, all that can be said is that the maximum possible $K_{Ii}/K_{Ic} = 1/a$, and that the cycles performed after the first cycle could have done some

needless damage to the vessel because of cyclic flaw growth. However, special circumstances occasionally dictate the need, or make it desirable, to conduct more than one proof test. The majority of the vessels used in the Apollo program use a single-cycle proof test.

2.2.2.7 Need for Postproof-Test Inspection

Current practice in industry regarding inspection after proof testing is divided, and there have been arguments made both for and against this inspection. There is general agreement that postproof-test nondestructive inspection can in some cases detect flaws which were previously missed (perhaps because the flaws were too tight) and detect flaw enlargement that may have occurred as a result of the proof test. Also, inspection after proof test can potentially point to areas of the vessel requiring process or design improvement. Considering this to be the case, the postproof inspection of at least the initial vessels fabricated from a new design appears desirable.

However, the discovery of flaws following a proof test can create a dilemma concerning the action required. If the flaws are repaired, another proof-test and postproof-test inspection are generally required. This cycle could conceivably be repeated several times before the vessel is (or appears to be) free of flaws. Furthermore, it is argued (and many times correctly so) that the multiple repairs can be more detrimental than the original flaws.

From the standpoint of fracture mechanics, there seems to be no particular need for postproof-test inspection if the proof test is properly designed and successfully executed. Any flaws that may be present after the test should not be of sufficient size to cause operational failure of the pressure vessel.

Based on pressure-vessel experience, there appears to be no strong arguments either for or against postproof-test inspection. Because the inspection in itself is not harmful, there is no reason to say that it should not be performed. However, it does appear that caution should be exercised to avoid over repair and reproof.

2.2.2.8 Need for Combined-Load Proof Tests

In most proof tests of pressure vessels, internal pressure is the only applied load. However, in some cases, vessels are critical for internal pressure combined with flight loads, and it is not possible to represent the operational stress levels in the vessel by internal pressure alone. In such cases, it generally appears desirable to include provisions in the test setup to apply representative flight loads combined with internal pressure. This has been done for some aerospace pressure vessels.

2.3 Subcritical Flaw Growth

Subcritical flaw growth can occur as a result of cyclic loading, sustained-stress loading, and combined sustained-stress and cyclic loading. When the sustained-stress flaw growth is environmentally induced, it is often termed stress corrosion; combined cyclic and sustained-stress growth is called corrosion fatigue when environmentally induced. Because of the potentially high rates of flaw growth, the problems of sustained-stress and combined cyclic and sustained-stress flaw growth are particularly important in the design of aerospace pressure vessels.

Data from fracture specimen tests can be used in a fracture mechanics analysis to predict the number of cycles or the time the vessel must be under sustained pressure for an initial flaw to grow to critical size. It has been shown (refs. 19 to 23) that for a given environment and cyclic loading profile, the time or cycles to failure depends primarily upon the magnitude of the initial stress intensity, K_{Ii}, as compared to the critical stress intensity, K_{Ic} [i.e., cycles or time to failure = $f(K_{Ii}/K_{Ic})$]. This is particularly significant, because, as pointed out in the previous section, the proof test provides a measure of the maximum possible K_{Ii}/K_{Ic} in the vessel.

During the past several years, cyclic and sustained-stress flaw-growth data have been obtained for a large number of different pressure vessel materials in a wide variety of environments. Although there are several methods of graphically presenting such data, probably the simplest and most useful are plots of K_{Ii}/K_{Ic} versus cycles to failure and K_{Ii}/K_{Ic} versus time to failure. Figure 8 shows typical K_{Ii}/K_{Ic} versus cycle data for

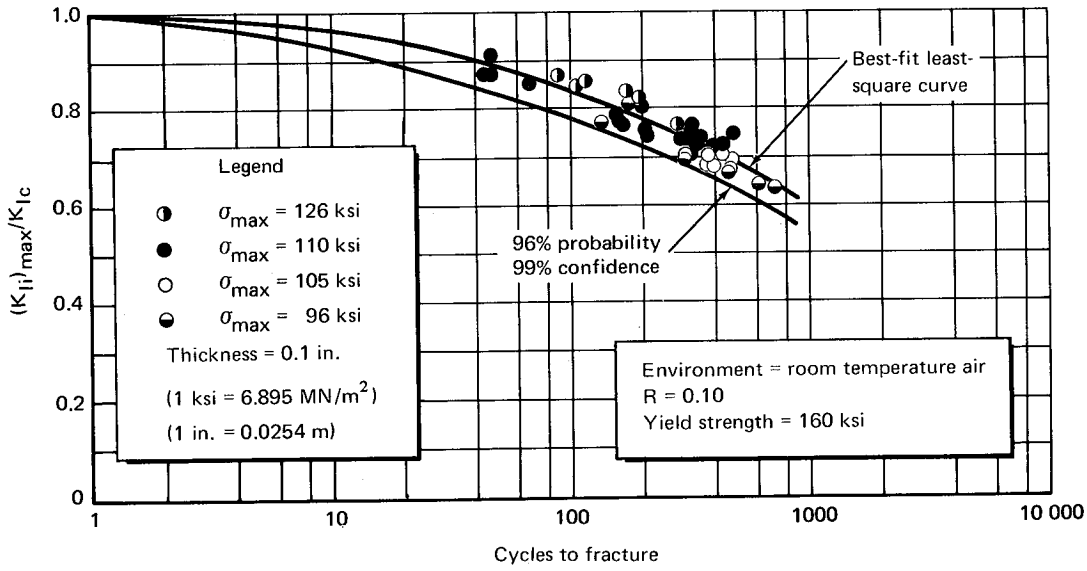

Figure 8. – Cyclic flaw-growth data for heat-treated 6Al-4V titanium.

6Al-4V titanium at room temperature. Both the best-fit curve and the 96-percent probability and 99-percent confidence-level curve are shown. Figure 9 shows K_{Ii}/K_{Ic} versus time data for 6Al-4V titanium in two different liquid environments. Experimental procedures used to obtain such cyclic and sustained-stress flaw-growth data are described in several references including references 18 to 23.

Several different types of test specimens have been used to obtain subcritical flaw-growth data. These include round notched bars, surface-flawed specimens, center-cracked panels, single-edge notched specimens, crack-line loaded specimens, and notched-bend specimens. Of major interest to the pressure-vessel designer is the growth of flaws under plane-strain conditions. Specimens containing through-cracks must be relatively thick, for most materials, to develop plane-strain conditions at the tip of the crack. This requirement has restricted the use of such specimens for the thin-walled pressure-vessel life prediction problem. On the other hand, such specimens have the advantage of permitting the observation and measurement of crack growth during the course of the test. Acquisition of these data has not been limited to any one type of specimen; however, the majority of the data on aerospace pressure vessel materials has been obtained with the surface-flawed specimen.

2.3.1 Sustained-Stress Flaw Growth

The most important characteristic observed in all sustained-stress flaw-growth experiments performed to date is the existence of a threshold stress-intensity level for a given material in a given environment. The observation has been that below a given

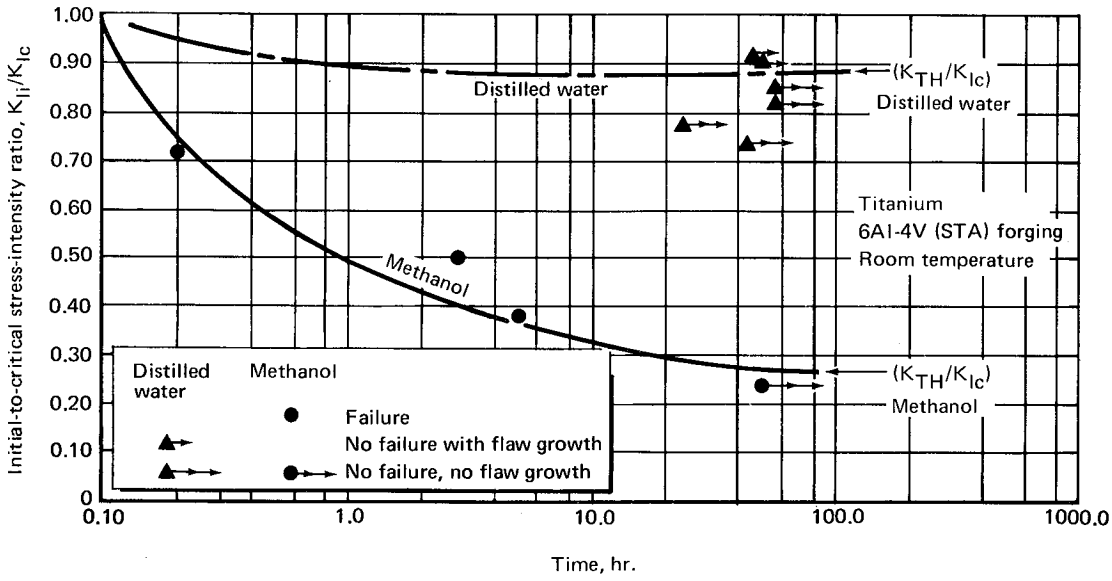

Figure 9. – Sustained-load flaw-growth data.

value of stress intensity, or K_{Ii}/K_{Ic} ratio, flaw growth has not been detected; above this value, growth does occur and can result in fracture. This stress intensity has been designated as K_{TH} and is shown in figure 9.

The discovery of a unique K_{TH} for a given material and environment is the key to the design of safe pressure vessels subjected to sustained loading. While K_{TH} can be 80 percent of K_{Ic}, or higher, in relatively inert environments, hostile media can reduce its value to less than one-half of K_{Ic} (fig. 9). In general, it has been found that K_{TH} values decrease with increasing yield strength in steel alloys (refs. 24 and 25). Also, there is considerable evidence indicating that sustained-load flaw growth is most severe under conditions of plane strain (ref. 26). Reference 27 shows that K_{TH} values, determined from tests of through-the-thickness cracked specimens, increase with decrease in specimen thickness.

Studies of flaw growth and stress intensity for materials in aggressive environments (refs. 25 to 31) indicate an ever increasing flaw-growth rate with increasing stress intensity; however, as shown in reference 7, the growth rate may be relatively constant over an appreciable range of stress intensities. In tests for K_{TH}, wide scatter is often encountered in the data. Also encountered are abnormally short times to failure and very marked dependence on environmental characteristics (media and temperature). Even minor changes in the chemical composition of the environment can significantly affect the K_{TH} value (refs. 21 and 22).

In chemically inert environments, the crack growth rate initially decreases with increasing stress intensity. If the initial-stress intensity is sufficiently low, the crack may halt. At higher stress intensities, the crack growth rate passes through a minimum value and then increases steadily until the crack becomes unstable. This flaw-growth behavior is reported by Johnson (ref. 24) for AM 350 steel in a purified argon environment.

This behavior is also noted in reference 20, where two threshold stress intensities were defined for 5 Al-2.5 Sn (ELI) titanium and 2219-T87 aluminum in the environments of room air, liquid nitrogen, and liquid hydrogen. One threshold stress intensity was defined as that value above which flaw growth to failure could be expected, and the other as the value below which there is no flaw growth. In between these two threshold stress intensities, small amounts of flaw growth can occur; however, the growth apparently arrests after a short time at load.

From these remarks, it is apparent that the service conditions must be carefully simulated when developing K_{TH} data for pressure vessel design. Some examples of experimentally determined K_{TH}/K_{Ic} ratios are shown in table I.

TABLE I. – TYPICAL THRESHOLD STRESS-INTENSITY DATA FOR VARIOUS MATERIAL/ENVIRONMENT COMBINATIONS

Material	Temp., °F [a]	σ_{ys}, ksi [b]	Fluid environment	$\frac{K_{TH}}{K_{Ic}}$	Ref.
6Al-4V (STA) titanium forging	RT [c]	160	Methanol	0.24	21
	RT	160	Freon M.F.	0.58	21
	RT	160	N_2O_4 (.30 % NO)	0.74	22
	RT	160	N_2O_4 (.60 % NO)	0.83	22
	RT	160	H_2O + sodium chromate	0.82	21
	RT	160	H_2O	0.86	21
	RT	160	Helium, air, or GOX	0.90	21
	RT	160	Aerozine 50	0.82	21
	90	160	N_2O_4 (.30 % NO)	0.71	22
	90	160	N_2O_4 (.60 % NO)	0.75	22
	105	160	Monomethyl-hydrazine	0.75	21
	110	160	Aerozine 50	0.75	21
6Al-4V titanium weldments (heat-affected zones)	RT	126	Methanol	0.28	21
	RT	126	Freon M.F.	0.40	21
	RT	126	H_2O	0.83	21
	RT	126	H_2O + sodium chromate	0.82	21
5A1-25 Sn (ELI) titanium plate	-320	180	LN_2 ($\sigma <$ proportional limit)	>0.90	20
	-320	180	LN_2 ($\sigma >$ proportional limit)	0.82	20
	-423	210	LH_2	>0.90	20
2219-T87 aluminum plate	RT	58	Air	0.90 [d]	20
	-320	66	LN_2	0.82 [d]	20
	-423	72	LH_2	>0.85 [d]	20
4330 steel	RT	205	Water	0.24	24
4340 steel	RT	>200	Salt water	<0.20	32
GTA welds:					
18Ni (200) steel	RT	200	Salt water spray	>0.70	33
18Ni (250) steel	RT	235	Salt water spray	>0.70	33
12Ni-5Cr-3 Mo steel	RT	170	Salt water spray	>0.70	33
9Ni-4Co-2.5C steel	RT	170	Salt water spray	>0.70	33
Inconel 718	RT	165	Gaseous hydrogen at 5000 psig	<0.25	34

[a] $°K = (5/9)(°F + 459.67)$.

[b] 1 ksi = 6.895 MN/m^2.

[c] Room temperature.

[d] No failure K_{TH}, some growth observed at lower values (ref. 10).

Probably the most convincing evidence that the stress-intensity factor, K, is the controlling mechanical parameter in sustained-stress flaw growth are the strong correlations obtained between various types of fracture test specimens and between test specimens and actual pressure vessels.

Beachem and Brown (ref. 35) explored this consistency using three different test specimen types:

1. The center-cracked plate.

2. The surface-flawed plate.

3. The precracked cantilever beam.

Using 4340 steel in a dilute NaCl solution, the same K_{TH} value was obtained for all three types of test specimens. The work of Smith, Piper, and Downey (ref. 28) provides additional evidence. They used center-cracked specimens to determine the threshold stress intensity for crack initiation with end loading, and crack arrest with wedge-force loading. For Ti-8A1-1Mo-1V alloy in $3\frac{1}{2}$ percent salt solution, the threshold stress intensity for crack initiation was 20 to 25 ksi$\sqrt{\text{in.}}$ (1 ksi$\sqrt{\text{in.}}$ = 1.099$\frac{\text{MN}}{\text{m}^2}\sqrt{\text{m}}$) and for crack arrest 20 to 22 ksi$\sqrt{\text{in.}}$. For end-loaded test specimens under constant load, both the stress-intensity factor and net section stress increase with increasing crack length; with wedge-force loading, the net section stresses increase whereas the stress intensity decreases with increasing crack length. The excellent agreement between initiation and arrest values of K_{TH} clearly shows that it is the stress-intensity parameter and not net section stress that is the controlling parameter in sustained-stress crack growth. Correlations between sustained-stress flaw growth in surface-flawed fracture test specimens and pressure vessels subjected to sustained pressurization are shown in references 10, 20, and 34.

In addition to comparisons of laboratory test specimen data to pressure-vessel data, there have been several instances where data from sustained-stress fracture-test specimens and fracture-mechanics analyses have been used to describe conditions leading up to service failures and to arrive at corrective actions. Examples of service failure analyses include: a 4330-steel hydraulic actuator that failed in a water environment as shown in references 2 and 32; titanium pressure-vessel failures in an N_2O_4 propellant environment shown in reference 36; and titanium pressure-vessel failures in a methanol environment shown in reference 21.

2.3.2 Combined Cyclic and Sustained-Stress Flaw Growth

The use of K_{Ii}/K_{Ic} versus cycle data to predict the life of thick-walled pressure vessels was first reported in the literature in reference 15. It indicated that if the maximum possible K_{Ii}/K_{Ic} in the vessel were known (i.e., from a successful proof test), the ordinate of a K_{Ii}/K_{Ic} versus cycles plot, such as that shown in figure 8, could be entered at the appropriate value of K_{Ii}/K_{Ic} and the predicted minimum number of cycles to fracture read from the abscissa. Experimental substantiation of this approach, based on tests of actual preflawed pressure vessels, was subsequently presented in references 10, 18, and 19. However, this approach was based on the assumption that the pressure vessel was cycled at a speed comparable to that used in generating the test specimen data or that cyclic speed was not important. In reference 2, it was hypothesized that for values of initial-stress intensity (K_{Ii}) below the sustained-stress, threshold-stress intensity value (K_{TH}), cyclic speed (or hold time at maximum load) probably would not affect the cyclic growth rate of flaws; but for values of K_{Ii} above K_{TH}, it could have a significant effect. In other words, the minimum cyclic life was limited by the number of cycles required to increase the value of K_{Ii} to the K_{TH} value, and above the K_{TH} level, failure could occur in one additional cycle if the hold time was sufficiently long. On a curve of K_{Ii}/K_{Ic} versus log cycles to fracture, this cyclic life is represented by the difference between the number of cycles at the ordinates of K_{Ii}/K_{Ic} and K_{TH}/K_{Ic}.

To date there are limited experimental data to substantiate this hypothesis. These data were developed for 2219-T87 aluminum and 5Al-2.5Sn(ELI) titanium in the relatively inert environment of liquid nitrogen and are shown in reference 20. When materials are subjected to more aggressive environments (i.e., those resulting in low K_{TH}/K_{Ic} values) there is considerable doubt regarding the general validity of the hypothesis. There are some data on 8Al-lMo-lV titanium in a salt-water environment that indicate cyclic frequency has no significant effect on flaw-growth rate at stress-intensity levels below K_{TH}. These data are shown in reference 37. On the other hand, recent investigations by Barsom (ref. 38) and Wei (ref. 37) have shown that for some material-environment combinations, both the environment and the cyclic frequency can affect the flaw-growth rates at values of stress-intensity below K_{TH}. For example, Barsom has shown that, for 12Ni steel in a salt water environment, cyclic growth rates of flaws are higher than in a dry environment and progressively increase with decreasing cyclic frequency (i.e., from 10 Hz to 0.1 Hz) at stress-intensity (K_{max}) levels less than K_{TH}. A complete explanation of this type of behavior has not been obtained; however, it is apparent that additional research on environmentally enhanced fatigue growth (i.e., corrosion fatigue) is required.

If it is necessary to use materials having low-threshold, stress-intensity values (less than 70- to 80-percent K_{Ic}) in the expected operating environment, it appears that the effect of environment and cyclic frequency on cyclic growth rates of flaws should be determined and the appropriate rates used to estimate the life of the pressure vessel. As previously mentioned, the minimum allowable cyclic life is limited to the number of cycles required to increase the value of the initial stress intensity K_{Ii} to the K_{TH} value.

The technique for using data on K_{Ii}/K_{Ic} versus cycles to fracture to estimate pressure-vessel life also depends on pressure-vessel wall thickness. For thick-walled vessels, the K_{Ii}/K_{Ic} curves can be used directly, as previously indicated. For thin-walled vessels, the task is somewhat more complicated. When the depth of a surface flaw becomes large with respect to the wall thickness of the vessel, the stress intensity is higher than that predicted by the original Irwin surface-flaw equation (ref. 4), and as a result, the subcritical flaw-growth rates will be higher and the total vessel life shorter than that obtained from K_{Ii}/K_{Ic} curves of the type shown in figure 8. (It should be noted that shallow surface-flaw test specimens were used in generating the basic K_{Ii}/K_{Ic} data.) The increase in stress intensity for long surface flaws and for semicircular surface flaws, which become deep with respect to the vessel's wall thickness, has been approximated by Kobayashi and Smith, respectively (Sec. 2.1). As indicated in reference 8 and shown in the example in Appendix B, for thin-walled vessels, it is necessary to use flaw growth-rate data and to account for the stress-intensity magnification of deep flaws when making estimates of vessel life. Curves of flaw-growth rate can be obtained by differentiating the curves of K_{Ii}/K_{Ic} versus cycle. For a given vessel design, the flaw growth-rate curves can then be arithmetically integrated using the Kobayashi approximation to account for the increase in stress intensity as the flaw approaches the free surface of the pressure-vessel wall. A relatively simple procedure is shown in reference 8. Like thick-walled vessels subjected to long hold times at maximum pressure, the cyclic life of thin-walled vessels is the number of cycles required to increase the stress intensity from some known or maximum possible initial value to the threshold value for sustained stress flaw growth.

In the analysis of thin-walled vessels, if it is found that the flaw gets very deep (i.e., approximately one plastic zone size from the back surface of the vessel wall) prior to attaining the threshold-stress intensity, it appears wise to experimentally determine cyclic flaw-growth rates with preflawed test specimens having the same thickness as the actual vessel wall. The plane-strain plastic zone size can be approximated by

$$\frac{\pi}{16}\left(\frac{K_I}{\sigma_{ys}}\right)^2 \tag{3}$$

Recent studies (ref. 39) have shown that in this situation the flaw-growth rates at a given stress-intensity level may be higher than those predicted from the results of shallow-flaw, thick-specimen test data.

The design objective is to assure that the minimum acceptable pressure-vessel life will be attained, rather than to estimate life per se. This can be accomplished from an accurate prediction of the service life by using laboratory cyclic and sustained-stress flaw-growth data to establish allowable K_{Ii}/K_{Ic} ratios, and by determining from these ratios the required proof-test factors and maximum permissible initial flaw sizes.

3. CRITERIA

Metallic pressure vessels for space vehicles shall be designed to avoid service failure caused by flaws and to ensure that the probability of catastrophic failure resulting from flaws during proof tests is remote. The pressures, temperatures, environments, and stresses from sources other than internal pressure to which the pressure vessels will be exposed shall be accounted for. The materials selected for pressure vessels shall possess appropriate fracture- and flaw-growth characteristics; and, all material properties or characteristics used in design and analysis shall be taken from reliable sources of data or adequately substantiated by tests. Critical flaw sizes for stress levels of interest shall be determined by analysis or test as appropriate. Where possible, the maximum size of initial flaws permitted in pressure vessels shall be sufficient to have a high probability of detection by nondestructive inspection but not sufficient to attain the critical flaw size during the pressure vessel's service life. In addition, the permissible initial flaw size shall be less than the critical flaw size at the proof-pressure stress level. The initial stress-intensity ratio permitted in pressure vessels shall be selected to ensure that the critical stress-intensity ratio is not attained during the design life of the vessel. Each pressure vessel shall be proof tested. The proof-pressure level shall be selected to demonstrate that the pressure vessel is free of flaws larger than the permissible initial flaw size or that the actual initial stress-intensity ratio is less than the permissible initial stress-intensity ratio. Account shall be taken of differences between the proof test and service temperatures, and of the time required to pressurize and depressurize the vessel during the proof test.

3.1 Design Conditions

The maximum operating pressure shall be determined for each pressure vessel, and the probability of exceeding this pressure during test (except proof test) and service usage

shall be sufficiently low to be consistent with the overall vehicle flightworthiness requirements.

The internal pressure-time-temperature history for the vessel during test, storage, and service use shall be determined.

The internal and external liquid and gaseous environments to which the vessel will be exposed during test, storage, and service use shall be determined.

Temperature gradients associated with all critical ground and flight conditions shall be determined and accounted for in the design and test of each metallic pressure vessel.

Stresses resulting from flight and ground loads shall be determined analytically and/or experimentally; if they occur simultaneously with and are additive to internal pressure stresses, they shall be accounted for in the design and simulated during the proof test of the vessel.

Local yielding caused by stresses resulting from design discontinuities and manufacturing discontinuities shall be permitted at the proof-test pressure level if empirical flaw size versus stress data have been obtained for the particular discontinuities in question (e.g., asymmetrical weld lands, mismatch, etc.) and if it has been demonstrated that at the proof-test pressure the flaw size required to cause fracture either exceeds the local material thickness or is of sufficient size to result in a high probability of detection. This procedure is necessary to minimize the probability of proof-test failure. General yielding shall not be permitted at the proof-pressure level unless the pressure vessel is designed to accommodate it.

3.2 Materials

The fracture and subcritical flaw-growth characteristics of the pressure vessel materials shall be determined for all critical environmental conditions.

Materials with low sustained-stress, threshold-stress intensity values in the anticipated service environment shall not be used in metallic pressure vessels unless adequate protection from the service environment can be demonstrated by test.

Material properties used in the design of metallic pressure vessels shall be the "A" values of MIL-HDBK-5 for unflawed parent metal or obtained in the same manner as those values.

Material properties of weldments and repaired weldments shall be obtained by tests based on the same procedure used in obtaining the "A" values of MIL-HDBK-5 for unflawed parent metal.

3.3 Critical Flaw Sizes

When the proof and maximum-operating stress levels are less than the tensile yield strength of the pressure-vessel material, the critical flaw sizes shall be calculated and based on the appropriate stress-intensity equations, the applied stress, and the measured plane-strain fracture toughness of the material.

When the applied stress (proof or operating) exceeds the tensile yield strength of the material, the critical flaw sizes shall be empirically determined using test specimens that contain flaws simulating those that could be encountered in the actual pressure vessel.

3.4 Initial Flaw Size

The maximum permissible initial flaw size in metallic pressure vessels shall be the largest flaw which cannot attain the critical flaw size within the required life span of the vessel, and shall be smaller than the critical flaw at the proof-stress level.

Pressure-vessel joints having the permissible radial and/or angular mismatch and containing the maximum permissible initial surface-flaw size on the high tension-stressed surface shall be capable of withstanding the proof stress without failure.

3.5 Allowable Stress-Intensity Ratio

The allowable initial-to-critical stress-intensity ratio for a metallic pressure vessel shall be the largest value which cannot attain unity within the required life span of the vessel.

The allowable initial-to-critical stress-intensity ratio shall be no higher than the value obtained from an analysis of the subcritical flaw-growth tests of the pressure-vessel materials in the anticipated service environments.

The allowable initial-to-critical stress-intensity ratio for metallic pressure vessels subject to short-time pressurization shall be allowed to exceed the threshold-to-critical stress-intensity ratio only if it can be shown by test that the allowable ratio cannot attain unity during the operational life of the vessel.

3.6 Proof Test

Each pressure vessel shall be subjected to a proof test. The proof-test factor shall be equal to, or greater than, one divided by the allowable initial-to-critical stress-intensity ratio.

When it has been shown by test that the pressure-vessel materials exhibit a decreasing fracture resistance with decreasing temperature, the proof test shall be conducted at a temperature equal to, or less than, the lowest expected operating temperature.

The pressurization time and hold time at the proof-pressure level shall be the minimum practical, consistent with possible test-system limitations. Emphasis shall be placed on minimizing depressurization time.

Analytical and experimental verification that the probable service failure mode is leakage rather than catastrophic fracture shall be required when assurance of safe operational life cannot be provided by proof test.

4. RECOMMENDED PRACTICES

From the discussion in Section 2 it is apparent that to prevent proof-test failures, low proof-stress levels and materials having high fracture-toughness values should be used so that the critical flaw sizes are large and hopefully exceed the thickness of the pressure-vessel wall. In this case the worst that could happen during proof testing is that the vessel would leak and require repair. Also, it is apparent that to obtain maximum assurance of safe operational performance it would be preferable to use large proof-test factors, low operational-stress levels, and materials with low flaw-growth rates under cyclic loads and high values of K_{TH} in the expected service environment. However, the use of high proof-test factors, low proof-stress levels, low operating-stress levels, and materials having very high fracture-toughness values (often associated with low tensile strengths) generally leads to excessively high pressure-vessel weight. With the possible exception of some first-stage launch-vehicle tankage, these vessels are generally not cost effective in terms of the delivery cost in dollars-per-pound of payload in orbit.

Tradeoffs can and should be made to arrive at an optimum design for a given pressure vessel application. The interrelations between materials, the required service life of the vessel, the required proof-test factor, the allowable flaw sizes, the probability of proof-test failure, and the weight of the pressure vessel should be understood and carefully assessed. These interrelations are illustrated in a simplified example in Appendix A. Tradeoffs, however, must be made within the constraints provided by the design criteria of the previous section.

4.1 Design Conditions

To prevent premature service failure of metallic pressure vessels, it is extremely important to consider the entire anticipated pressure-time-temperature history of the vessel and the environments to which it will be exposed.

The value of maximum operating pressure used in the design of liquid propellant tanks and gas bottles should equal the maximum nominal-operating pressure plus the upper tolerance of the pressure-limiting device. This device should have a reliability consistent with the overall vehicle flightworthiness requirements.

The predicted pressure-vessel history should include pressures, times, temperatures, and fluid and gaseous environments for all of the anticipated cycles, starting with the initial proof-pressure test and ending with the last service-pressure cycle. Also, it is important to include pressurization rates, depressurization rates, and hold times. In those cases where the life history of the vessel cannot be accurately predicted, a design life envelope should be established and the appropriate operational limitations placed upon the completed vessel.

Loads other than internal pressure, such as slosh, sonic, vibration, handling, and transportation loads, should be determined in accordance with applicable NASA monographs. Effort should be made to minimize high stresses resulting from flight and ground loads by careful detailed design and by using antislosh, damping, and antishock devices. Stresses resulting from external flight and ground loads should be determined analytically and/or experimentally, and accounted for in the design of the pressure vessel. Temperature gradients (and resulting thermal stresses) should be determined for all critical ground and flight conditions. If the stresses are of sufficient magnitude to affect the basic vessel design, an effort should be made to minimize or eliminate these stresses using thermal insulation, controlled fill rates of cryogens, etc.

Wherever possible, the objective should be to eliminate residual stresses by stress relief treatments. If this is not practical, residual stresses should be minimized by careful design and controlled welding procedures.

A stress analysis should be performed for every vessel and include stresses resulting from internal pressure, ground and flight loads, and thermal gradients. The analysis of stresses resulting from internal pressure should include primary membrane stresses and secondary bending and membrane stresses that result from design discontinuities and allowable design deviations.

General yielding should be avoided during pressure testing except for those vessels that are specifically designed to accommodate it (e.g., cryoformed stainless-steel vessels). To

avoid general yielding during proof-pressure testing, the minimum design ultimate factor of safety, $(F.S.)_{MDU}$, should be as follows:

$$(F.S.)_{MDU} = a \times \frac{\text{Parent metal ultimate strength}}{\text{Parent metal yield strength}} \quad (4)$$

Where

a = Proof factor = $1 \div (\text{Allowable } K_{Ii}/K_{Ic})$

The factors previously specified are minimum values for all metallic pressure vessels used on both manned and unmanned vehicles. Uncertainties in loads, pressures, service environments, and/or service requirements may make it necessary to use higher factors; however, in no case should lower factors be used.

4.2 Materials

The following fracture and subcritical flaw-growth characteristics should be obtained for materials intended for use in metallic pressure vessels:

1. The plane-strain fracture toughness values (i.e., K_{Ic} values) for the parent metal, weldments, and heat-affected zones at the operating- and proof-test temperatures, and in the principal directions of loadings.

2. The threshold stress-intensity (K_{TH}) values for the parent metal, weldments, and heat-affected zones in simulated service environments.

3. The cyclic flaw-growth data (curves of K_{Ii}/K_{Ic} versus cycles or $\frac{d(\frac{a}{Q})}{dN}$ versus K) for the parent metal, weldments, and heat-affected zones.

In addition, the effects of material processing on these fracture characteristics should be determined. A quality control program should be established to determine that large variations in values of toughness or threshold stress-intensity ratios do not occur from one batch, or heat, of material to another. Also, each manufacturing process that might adversely affect the strength, toughness, and threshold stress-intensity values of the end product (e.g., welding and heat treating) should be certified by performing specimen tests. Test specimens should have the same shape, be made from the same materials, and use the processes planned for production hardware.

The quantity of fracture test data obtained should be determined on the basis of the impact a failure would have on the mission, schedules, and costs.

To comply with the criteria in this monograph, it is unnecessary to limit the determination of fracture toughness values to any particular type of test specimen. However, it does appear that the curves of predicted critical flaw size (based on the measured K_{Ic} values) for the pressure-vessel parent metal, weldments, and heat-affected zones should be verified by data from a series of surface-flawed specimen tests. The test specimens should be the same thickness, processed in the same manner as the vessel, and each should contain a different size flaw. Procedures for specimen fabrication and test are discussed in reference 19. To eliminate the effects of inplane bending and specimen width, the test-specimen width should be about five times the surface-flaw length (i.e., the 2c dimension).

Likewise, the acquisition of threshold stress-intensity (K_{TH}) data and cyclic flaw-growth data should not be limited to the use of any one type of test specimen. However, the surface-flawed specimen has been used to obtain the majority of such data to date (Sec. 2).

The recommended experimental approaches for using surface-flawed test specimens to obtain data on K_{Ii}/K_{Ic} versus cycles, and K_{Ii}/K_{Ic} versus time are described in references 19 to 23; therefore, it is unnecessary to repeat the approaches in detail in this monograph, however, the following deserve particular attention.

Data on cyclic and sustained-stress flaw growth should be obtained for parent metal, weldments, and heat-affected zones. The test specimens should be of sufficient width to prevent inplane bending effects; for the cyclic tests, it is particularly important that the test specimen be sufficiently thick to ensure that the flaw attains the critical size before growing more than half way through the thickness of the specimen. It is also recommended that cyclic tests be performed in the anticipated service environment and that the effect of cyclic frequency be evaluated. In most cases, a cyclic frequency of about 0.0167 to 0.0833 Hz (1 to 5 cpm) is considered suitable. For the sustained-stress tests accurate simulation of the anticipated service environment should be emphasized. A complete set of data on K_{Ii}/K_{Ic} versus cycle should be obtained for each of the anticipated service-loading profiles (i.e., R values). It is conceivable that in some cases prior load, temperature, and environment histories could have a detrimental effect on cyclic- and sustained-stress, flaw-growth characteristics. If this is suspected, the effects should be determined experimentally.

The required fracture-toughness and subcritical flaw-growth characteristics of materials to be used in metallic pressure vessels cannot be specified in terms of specific minimum or maximum allowable values because of the many factors involved. However, in general, it is recommended that the material have sufficient fracture toughness so that the predicted critical flaw sizes at the applied proof stress are sufficiently large so that there is a high probability of their being detected prior to the test. Also, materials that

exhibit a low-threshold stress intensity in the anticipated service environment should be avoided. If the material has a K_{TH} value below about 70 percent of K_{Ic}, the possible use of alternate materials should be investigated.

Use of the improvements in allowable uniaxial ultimate and yield strengths caused by biaxial stress fields results in increased operational and proof stresses as well as lighter weight pressure vessels. The higher stresses reduce the critical flaw sizes, however, and increase the chances of premature failure of the pressure vessel. Therefore, increases in the allowable uniaxial tensile yield and ultimate strengths of parent metal caused by biaxial stress should be taken into account only if

1. The critical flaw sizes associated with the increased proof-stress level are large (high probability of being detected prior to the test).

2. Sufficient experimental data are available to allow a reliable determination of the biaxial improvement factor.

Because of the high probability of the occurrence of defects and the complexities in stress fields introduced by design and manufacturing discontinuities, biaxial strength elevation should not be used to establish allowable ultimate strengths of welded joints.

In cases where the effect of the biaxial stress field reduces the uniaxial tensile strength, the amount of the reduction should be determined experimentally and used to establish allowable strengths.

4.3 Critical Flaw Sizes

Prevention of proof-test failure requires knowledge of the critical flaw sizes at proof-stress levels, knowledge of possible flaw growth during proof test, and detection and repair of all flaws that exceed or could attain the critical size during proof test. Prediction of accurate critical flaw sizes is not always an easy task; however, it is a necessary goal.

The concept of critical flaw sizes and the equations for determining these sizes for surface flaws in thick- and thin-walled vessels were introduced in section 2. These equations apply, however, only when the gross stress levels of the pressure vessel are below the yield strength of the pressure-vessel material and when the stresses are uniform through the thickness of the vessel wall. When this is the case (as in areas of a vessel that are under membrane stress), it must be recognized that the accuracy of the calculated critical flaw size depends directly on how accurately the material's fracture toughness (K_{Ic}) and the applied stress levels are known. When calculating critical flaw

sizes for these areas of uniform elastic stress, the value of K_{Ic} selected for design and the maximum possible applied stress level (i.e., that corresponding to the minimum material gage) should be used. In addition, it is a conservative viewpoint to assume that the flaws are surface (or just subsurface) flaws and that they are long in relation to their depth so that $Q \approx 1.0$. The resulting predicted critical flaw size is thus described by the single dimension, a (i.e., the depth). When this depth is large with respect to the wall thickness (i.e., greater than about half the thickness), the effect of deep-flaw stress-intensity magnification should be accounted for. The equation shown in figure 3 attempts to do this by the addition of the M_K factor. A reasonable estimate for M_K is the approximate Kobayashi solution shown in figure 3. While recent data (ref. 39) indicate that its use can result in somewhat conservative answers for the more ductile materials and perhaps slightly unconservative answers for the brittle materials, it is recommended that the figure 3 curve be used until improved solutions are obtained. Since the equation shown in figure 3 is not explicit in terms of the critical flaw size, various critical depths (a_{cr}) should be assumed for the long surface flaw, the M_K values determined from the Kobayashi curve, and the failure stresses calculated. The curve of σ versus a_{cr} can then be plotted. If the a_{cr} at the proof- (or operating-) stress level is larger than the wall thickness, the expected failure mode for the vessel at proof- (or operating-) pressure would be leakage. However, this can be predicted with confidence only if there are no higher stressed areas in the vessel where the critical flaw depth would be smaller, or if the value calculated for a_{cr} exceeds the wall thickness by a significant amount.

In most vessels there are areas where the stresses are not uniform through the thickness of the wall (i.e., at mismatched weld joints, asymmetrical weld lands, changes of contour, etc.) and many times it is known that at the proof pressure the total applied stresses in these local areas exceed the yield strength of the material. If it is known that the stresses approach or exceed the material yield strength, an estimate of the critical flaw sizes (for long surface flaws) may be made by test. For these cases, the critical flaw-size data should be obtained by testing a series of surface-flawed specimens (with various size flaws) that model the actual hardware. It is further recommended that the flaws be made long in relation to their depth (i.e., small a/2c ratios) and that the specimen width be about five times the flaw length.

In areas of nonuniform stress (e.g., combined bending plus tension) where the stresses are within the elastic range, it is possible to make reasonably accurate estimates of the critical flaw sizes by analysis. References 6 and 40 present both approximate and numerically exact stress-intensity solutions for nonuniform stress fields. Also, there are often special situations (particularly during the failure analysis studies or Material Review Board type actions) where it is of interest to predict critical sizes (or failure stresses) for flaws of shapes, locations, or orientations other than those previously

discussed. For example, corner flaws, near-surface internal flaws, coplanar-internal flaws, and sharp-tailed porosity may all be encountered. Again, for most of these situations, reasonably accurate analytical estimates can be made (providing the stress field is elastic) using various available stress-intensity solutions. Some such solutions are included in references 2, 6, 41, and 42. Others are currently being developed.

4.4 Initial Flaw Size

The two distinct areas of concern regarding initial flaw sizes are as follows:

1. The determination of either actual or maximum possible initial flaw sizes in the vessel as initially fabricated, and before and after the proof test.

2. The determination of maximum permissible initial flaw sizes (i.e., the allowable initial flaw sizes) before the proof test.

Nondestructive inspection (i.e., X-ray, ultrasonic, etc.) is the only means for determining actual initial flaw sizes before the proof test (Sec. 2), consequently, such inspections should be used to minimize the possibility of proof-test failure. The extent of nondestructive inspection should be determined on an individual basis, taking into consideration the consequences of a proof-test failure, the capabilities of the available inspection techniques, and the sizes of initial flaws that must be detected (i.e., the allowable initial flaw sizes).

The successful proof test provides a direct measure of the maximum possible initial-to-critical stress-intensity ratio to predict the specific maximum possible initial flaw sizes that may exist in the vessel after the proof test and before the service usage. (Due to possible flaw growth during the proof test, the initial flaw sizes before and after the proof test may not be the same). If the proof test is properly designed and successfully executed, the maximum possible initial flaw sizes after the proof test are equal to the predicted critical flaw sizes at the proof-stress level. However, since the proof test itself provides assurance against operational failure, the prevention of such failure does not require the prediction of allowable initial flaw size.

Allowable initial flaw sizes should be determined for the following specific purposes:

1. Assessing the adequacy of the nondestructive inspection procedures.

2. Assessing the adequacy of the flaw or defect acceptance limits.

3. Assessing the probability of a proof-test failure.

These require that the allowable initial flaw sizes be established for all high-stressed areas of the vessel, including the parent metal, weldments, and heat-affected zones.

The allowable initial flaw sizes should be established using the allowable initial-to-critical stress-intensity ratios determined from subcritical flaw-growth test data (Sec. 4.5); the measured K_{Ic} values for the parent metal, welds, and heat-affected zones; experimental measurements of possible flaw growth that could occur during proof test; and the appropriate stress-intensity equations for various flaw-geometry and boundary-stress conditions. The same stress-intensity equations used in predicting critical flaw sizes (Sec. 4.3) should be used to establish allowable initial flaw sizes except to substitute the allowable value of K_{Ii} for K_{Ic}.

4.5 Allowable Stress-Intensity Ratio

The allowable initial-to-critical stress-intensity ratio (i.e., allowable K_{Ii}/K_{Ic} ratio) is an important element in the control of fracture of metallic pressure vessels. Consequently, extreme care should be exercised in selecting the values of this ratio to be used in establishing the proof-test factor and the allowable initial flaw sizes. The allowable K_{Ii}/K_{Ic} ratio to be used in determining the proof-test factor (Secs. 3.2 and 4.1) should be a statistically meaningful value obtained from an analysis of the subcritical flaw-growth test data in the various anticipated service environments for the parent metal, welds, and heat-affected zones. When allowable K_{Ii}/K_{Ic} ratios are used to establish allowable initial flaw sizes, the value of K_{Ii}/K_{Ic} for the specific area of interest of the vessel should be used. Also, the selected design value of K_{Ic} should be used.

The allowable K_{Ii}/K_{Ic} ratio should be determined, using statistically meaningful curves of subcritical flaw growth (i.e., K_{Ii}/K_{Ic} versus cycle and K_{Ii}/K_{Ic} versus time) and the most severe service history anticipated for the vessel (Sec. 4.1).

The flaw-growth curves should take into account possible heat-to-heat variations in the values of K_{TH} and K_{Ic} and the scatter in these values within a given heat. References 22 and 43 present discussions on the effects of data scatter and heat-to-heat variations.

Complexity of the analysis required to determine allowable K_{Ii}/K_{Ic} ratios depends upon the pressure-vessel design and the complexity of the anticipated service history. A recommended procedure for performing this analysis can best be illustrated by specific examples for thick- and thin-walled vessels. These examples are presented in Appendix B.

4.6 Proof Test

Every pressure vessel should be proof tested to a stress level equal to or greater than the maximum operating stress times a ($a = 1 \div$ allowable K_{Ii}/K_{Ic}). If the vessel is proof tested at a temperature other than the operating or service temperature, the minimum proof-test factor, a, should be determined by equation (2) in Section 2.

In this case, it is important that the values of K_{Ic} are known for all areas of the vessel and that it is known how they vary as a function of temperature. Also, it is important to know the probable scatter in values of K_{Ic} at both the operating and proof-test temperature. To ensure that the proof-test factor obtained will be adequate, the upper statistical value of the K_{Ic} scatter band at the proof-test temperature and the lower statistical value at the operating temperature should be used.

The proof test should be conducted with a test fluid that will neither induce general corrosion pitting nor severe stress-corrosion cracking. The values of K_{TH} for the vessel materials should be obtained from sustained-stress fracture tests performed in the test fluid at the proof-test temperature. If the values of K_{TH} are low, either an alternate fluid should be selected or, if this is not practical, methods of protecting the vessel or inhibiting the action of the test fluid should be investigated.

Slow flaw growth during pressurization and elapsed time at proof pressure should be minimized by rapid pressurization rates and short hold times. The pressurization time should be the minimum possible, consistent with the capabilities of the test equipment. A maximum hold time of about 15 seconds is considered to be reasonable.

It is extremely important to minimize the time necessary to depressurize from the proof pressure to a pressure equal to K_{TH}/K_{Ic} times the proof pressure. If this cannot be accomplished in a few seconds because of test-system limitations or the pressure-vessel design, the potential detrimental effects of the slower depressurization should be determined by analysis. An illustrative example of a recommended analysis procedure is shown in reference 7.

Proof testing of metallic pressure vessels should be limited to a single pressure cycle unless there are special circumstances indicating the need for additional cycles. Special circumstances include the following cases:

1. A single proof test cannot be designed to envelop the critical operational pressure, temperature, and external loading combinations.

2. The vessel was modified or repaired after the initial proof test and the modified or repaired areas of the vessel need to be proof tested.

3. It is desired to recertify the vessel for additional service usage after it has been in service for a period of time.

4. From an economical standpoint, it is desired to test components (e.g., bulkheads) of the vessel prior to final assembly.

5. It has been shown by laboratory experiments on preflawed simulated parts or specimens that a prior test at a higher temperature is advantageous to minimuze the risk of failure at the design temperature.

A failure-mode analysis should be performed for each completed pressure-vessel design. The predicted failure mode (i.e., leakage or complete fracture) should be determined at the proof and maximum operating conditions.

Analytical and experimental verification that the probable failure mode is leakage rather than complete fracture should be obtained in cases where assurance of operational life is not provided by the proof test.

For those pressure vessels which are critical for internal pressure combined with flight loads, it may not be possible to represent the operational stress levels in the vessel by internal pressure alone. In such cases, the proof test should include provisions to apply representative flight loads combined with internal pressure.

APPENDIX A

DESIGN TRADE-ILLUSTRATIVE EXAMPLE

Figure A-1 illustrates how the various factors affecting reliability and weight are interrelated for pressure vessels designed to contain liquid hydrogen. In the upper portion of the figure, the cyclic lives of two materials are shown as a function of the inverse of the stress-intensity ratio (K_{Ii}/K_{Ic}). The cyclic growth of initial defects or flaws in a vessel is primarily a function of this ratio. Also, it can be shown that the maximum possible K_{Ii}/K_{Ic} ratio in a pressure vessel after a successful proof test is equal to 1 divided by the proof-test factor, a, or $K_{Ic}/K_{Ii} = a$. The solid lines are based on the assumption of rapid pressure cycling where the sustained-stress flaw growth above K_{TH} is negligible. The dashed lines are based on the assumption that there are long-duration hold times at maximum pressure; and, consequently, the life is the number of cycles required for the applied stress intensity to reach K_{TH}.

In the center portion of the figure, constant flaw-size lines are shown as a function of the proof-test factor and the square of the ratio of the plane-strain fracture toughness, K_{Ic}, and the operational stress level σ_{op}. These curves were obtained as follows:

$$K_{Ic} = 1.95\, \sigma_{proof}\, (a/Q)^{\frac{1}{2}}_{cr_{proof}} \tag{A-1}$$

however:

$$\sigma_{proof} = a\, \sigma_{op}$$

$$\max (a/Q)_{i_{op}} = (a/Q)_{cr_{proof}}$$

substituting:

$$K_{Ic} = 1.95\, a\, \sigma_{op}\, (a/Q)^{\frac{1}{2}}_{i}$$

$$\left(\frac{K_{Ic}}{\sigma_{op}}\right)^2 = 3.8\, a^2\, (a/Q)_i \tag{A-2}$$

With $(a/Q)_i$ held as a constant, the equation can be solved and plotted in terms of $(K_{Ic}/\sigma_{op})^2$ vs a.

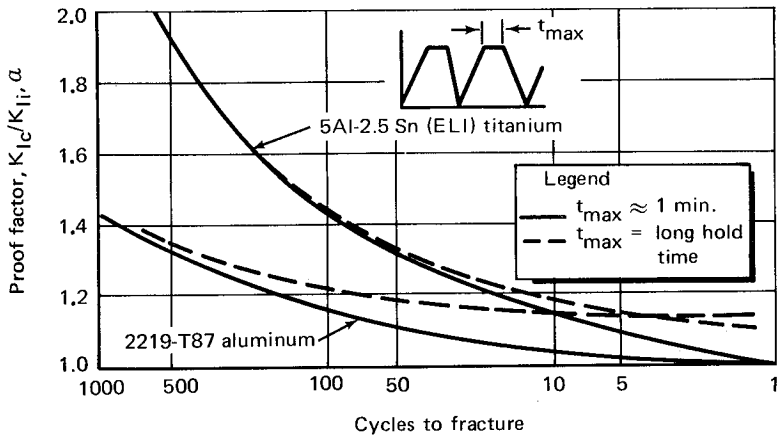

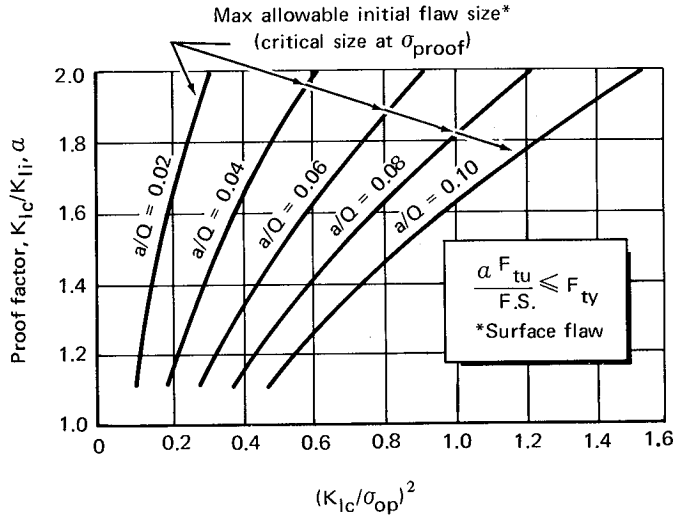

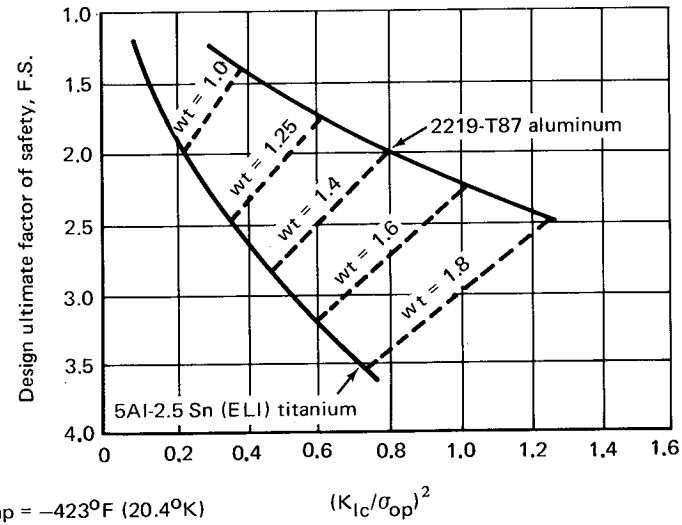

Design temp = −423°F (20.4°K)

Figure A-1. – Interrelated factors affecting the weight and reliability of thick-walled LH_2 pressure vessels.

The lower portion of the figure shows the relationship between the design ultimate factor of safety (F.S.) and $(K_{Ic}/\sigma_{op})^2$ for the two materials, obtained from the following relationship:

$$\left(\frac{K_{Ic}}{\sigma_{op}}\right)^2 = \left(\frac{K_{Ic}}{\frac{\sigma_{ult.}}{F.S.}}\right)^2 = (F.S.)^2 \left(\frac{K_{Ic}}{\sigma_{ult.}}\right)^2 \qquad \text{(A-3)}$$

Points of equal pressure-vessel weight were computed for the aluminum and titanium, and connected by dashed lines with the relative weight indicated.

Consider a typical design problem: suppose it were desired to design a high-pressure helium vessel to be contained within a larger LH_2 propellant tank and have a required minimum life of 500 pressure cycles. From the upper portion of the figure it can be seen that a successful proof test to 1.95 times the maximum operating pressure would be required to assure this life using the titanium alloy, and 1.35 times the maximum operating pressure using the aluminum alloy. It should be noted that the 1.95 factor is somewhat higher than the conventional proof factor usually specified for high-pressure gas bottles and the 1.35 factor is lower than that usually specified. Suppose it were decided to use a conventional ultimate factor of safety of 2.5, commonly used for high-pressure bottles. From the lower portion of the figure it can be seen that $(K_{Ic}/\sigma_{op})^2$ equals 0.35 for the titanium and 1.25 for the aluminum. Also, it is seen that the weight of the aluminum vessel will be 1.8/1.25 or 1.44 times the weight of the titanium vessel. In the center portion of the figure, the flaw sizes that will cause failure during proof test can be determined. For the titanium vessel this is slightly greater than 0.02 in. (1 in. = 0.0254 m) (i.e., the depth of a long surface flaw) and for the aluminum vessel it is $>>$ 0.10 in.

It is doubtful if the titanium tank could successfully pass the proof test because of the difficulty in detecting an initial flaw size as small as the critical flaw size at the proof stress. On the other hand, this does not appear to be a problem with the aluminum tank. The use of the conventional factor of safety of 2.5 seems to unduly penalize the aluminum tank (i.e., causes it to be excessively heavy), and yet it is marginally adequate for the titanium tank.

If an aluminum tank were designed with an ultimate factor of safety of about 1.75, its weight would be equal to that of the titanium tank designed with an ultimate factor of safety of 2.5, and the critical flaw size at the proof-stress level (1.35 times σ_{op}) would be about 0.09 in. This flaw is still about four times larger than that for the titanium vessel and is sufficiently large to create some degree of confidence that all initial flaws,

equal to or greater than this size, will be detected by nondestructive inspection. As a result, proof-test failures (and the resulting high costs) should not be as probable as with the titanium vessel.

From the foregoing example it is apparent that using standardized design factors does not assure optimum (nor in some cases even adequate) designs. To preclude the possibility of failure of hazardous vessels, high factors of safety have often been specified. However, to save weight (caused by the high factors of safety) the designer has been forced to use higher strength (and generally lower toughness) materials. As a result, the risk of failure has often been increased rather than reduced.

While it can be argued that standardized factors of safety have been adequate for many past applications, the designer must concern himself not with average behavior, but with the exception which can result in failure. During recent years there have been costly exceptions.

APPENDIX B
ALLOWABLE STRESS-INTENSITY RATIO - ILLUSTRATIVE EXAMPLES

B.1 Thick-Walled Pressure Vessel

Suppose it is anticipated that a thick-walled 6Al-4V titanium helium tank will go through the preflight service history shown in figure B-1. The maximum design operating stress is σ_{op} and R is the ratio of minimum-to-maximum stress during a cycle. The following is a tabulation of the preflight history:

1. 200 loading cycles with the maximum stress = 90 percent of σ_{op} and R = 0.1.

2. 4300 loading cycles with the maximum stress = σ_{op} and R = 0.7.

3. 260 loading cycles with the maximum stress = 95 percent of σ_{op} and R = 0.4.

4. 60 loading cycles with the maximum stress = σ_{op} and R = 0.1.

5. A long-duration flight cycle with the maximum stress = σ_{op}.

To design an adequate proof test for this vessel, it is necessary to determine the maximum allowable K_{Ii}/K_{Ic} ratio and then to calculate the minimum proof-test factor.

The cyclic life curves for 6Al-4V titanium (STA) are reproduced in figure B-2 for R = 0.1 and R = 0.4, and R = 0.7 from reference 22. The change in K_{Ii}/K_{Ic} throughout the life of the titanium tank is graphically illustrated in figure B-2 and determined by the following procedure.

Because the value of threshold stress intensity for sustained-stress flaw growth is 90 percent of K_{Ic} (table I), the allowable value of K_{Ii}/K_{Ic} at the beginning of the long-duration flight cycle at σ_{op} is 0.90. This requirement is illustrated by point A in figure B-2.

The 60 loading cycles at σ_{op} and R = 0.1 change the K_{Ii}/K_{Ic} ratio from point A to point B in figure B-2. Point B is 60 cycles to the right of point A, with the cycles being measured along the abscissa of the plot of R = 0.1. Hence, the allowable K_{Ii}/K_{Ic} ratio at the beginning of the 60 cycles (point B in figures B-1 and B-2) is 0.84.

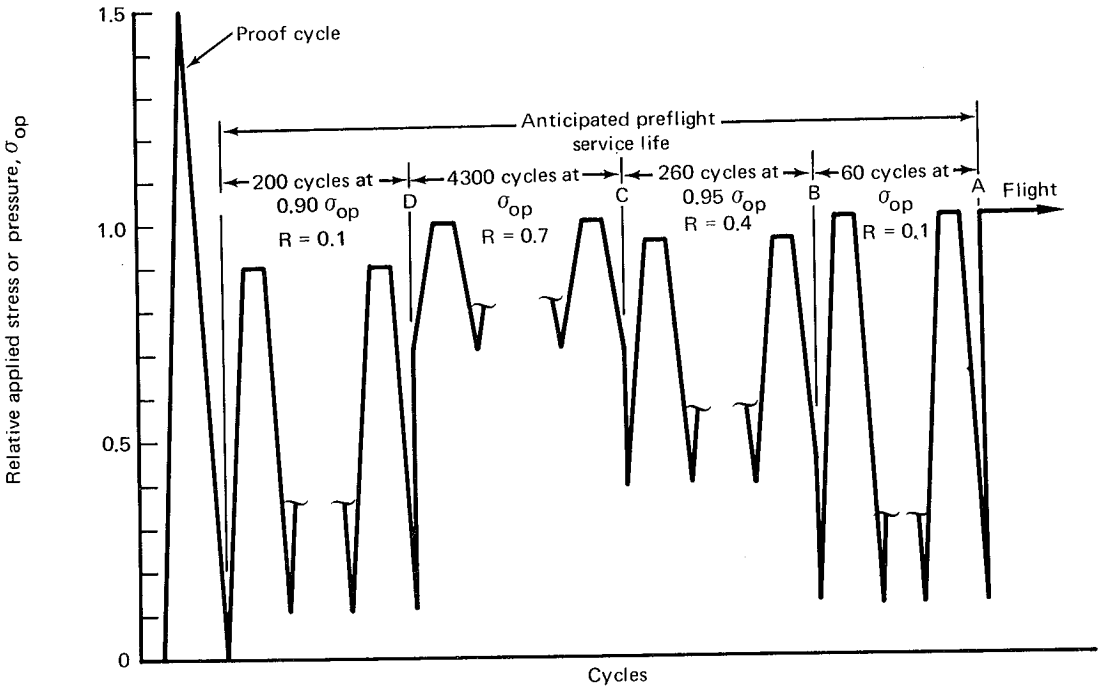

Figure B-1. – History of cyclic stresses of a thick-walled vessel.

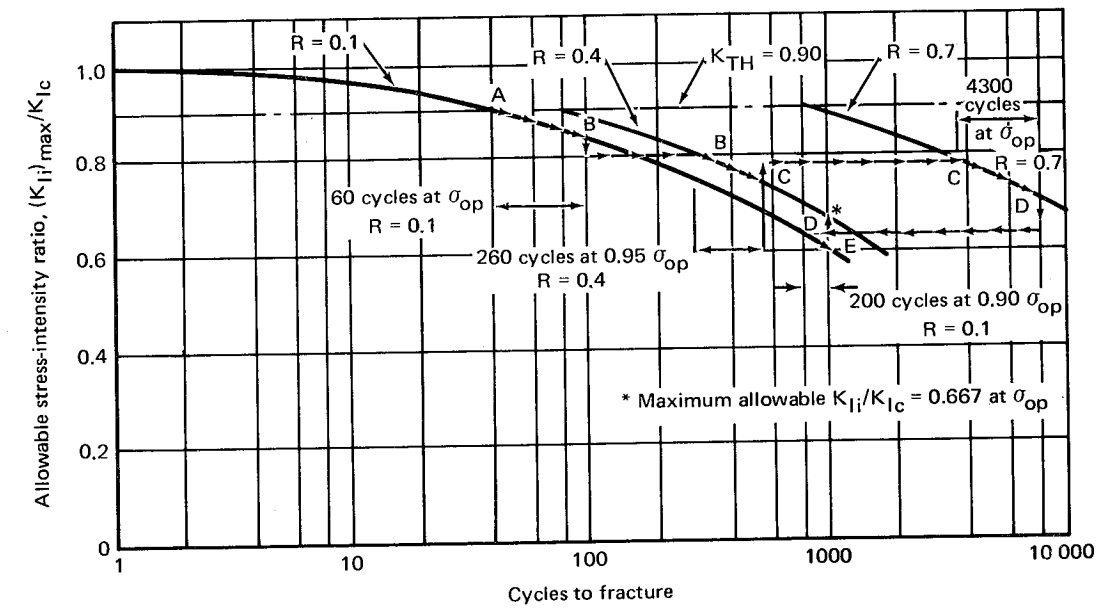

Figure B-2. – Determination of allowable stress-intensity ratio for a thick-walled vessel.

K_{Ii}/K_{Ic} is proportioned to the stress level (σ) because

$$K_{Ii}/K_{Ic} = \frac{1.1\sqrt{\pi}\ \sigma\ (a/Q)^{\frac{1}{2}}}{K_{Ic}} \qquad \text{(B-1)}$$

The stress level is 5 percent lower at the end of the 260 cycles than at the beginning of the 60 cycles, and since the flaw size is the same for both stress levels at that point (point B in figure B-1), then the allowable value of K_{Ii}/K_{Ic} at the end of the 260 loading cycles is (0.95/1.00) times 0.84 = 0.798. This K_{Ii}/K_{Ic} ratio is given by point B in figure B-2 on the R = 0.4 curve.

The 260 loading cycles with the maximum stress = 0.95 σ_{op} and R = 0.4 change the K_{Ii}/K_{Ic} ratio from that given by point B to that given by point C in figure B-2. Point C is 260 cycles to the right of point B on the plot of R = 0.4. Hence, the allowable K_{Ii}/K_{Ic} ratio at the beginning of the 260 cycles (point C in figures B-1 and B-2) is 0.74.

The stress level is 5 percent higher at the end of the 4300 cycles than at the beginning of the 260 cycles and, by the same reasoning given above, the allowable value of K_{Ii}/K_{Ic} at the end of 4300 cycles is (1/0.95) times 0.74 = 0.78. This K_{Ii}/K_{Ic} ratio is given by point C in figure B-2 on the R = 0.7 curve.

The 4300 loading cycles at σ_{op} and R = 0.7 change the K_{Ii}/K_{Ic} ratio from point C to point D in figure B-2. Point D is 4300 cycles to the right of point C on the plot of R = 0.7. Hence, the allowable K_{Ii}/K_{Ic} ratio at the beginning of the 4300 cycles (point D in figs. B-1 and B-2) is 0.70.

The stress level is 10 percent lower at the end of the 200 cycles than at the beginning of the 4300 cycles and therefore the allowable value of K_{Ii}/K_{Ic} at the end of the 200 cycles is (0.90/1.00) times 0.70 = 0.63. This K_{Ii}/K_{Ic} ratio is given by point D in figure B-2 on the R = 0.1 curve.

The 200 loading cycles with the maximum stress at 0.90 σ_{op} and R = 0.1 change the K_{Ii}/K_{Ic} ratio from that given by point D to that given by point E in figure B-2. Hence, the allowable K_{Ii}/K_{Ic} ratio at the beginning of the 200 cycles (point E in figs. B-1 and B-2) is 0.6. The operating stress is 10 percent higher than the stress at the beginning of the 200 cycles so that the allowable value of K_{Ii}/K_{Ic} at the operating stress is (1.0/0.9) times 0.6 = 0.667. This is shown by the asterisk in figure B-2.

Thus, for the pressure vessel subjected to the anticipated service history given, the maximum allowable K_{Ii}/K_{Ic} ratio at the end of the proof cycle is 0.667 and the minimum required proof-test factor is $a = 1/0.667 = 1.5$. This indirectly imposes a restriction on the maximum allowable operating stress because the proof stress should not exceed the yield strength of the material. Hence, the maximum allowable operating stress is 0.667 times σ_{ys}.

B.2 Thin-Walled Pressure Vessel

Suppose a thin-walled 6Al-4V (STA) titanium propellant tank designed to contain N_2O_4 at room temperature is expected to withstand a preflight service history, graphically shown in figure B-3, and tabulated as follows:

1. 20 loading cycles with maximum stress = 95 percent of the maximum design operating stress, σ_{op}.

2. 9 loading cycles with maximum stress = σ_{op}.

3. 20 loading cycles with maximum stress = 89 percent of σ_{op}.

4. A long-duration flight cycle with maximum stress = σ_{op}.

In the thin-walled tank, the flaw depth becomes deep with respect to the wall thickness of the tank before reaching the critical size. Hence, the stress-intensity factor must be corrected for the a/t ratio according to figure 3. Suppose the thickness of the tank wall is 0.022 in. (1 in. = 0.0254 m) and the maximum design operating stress, σ_{op} is 84.4 ksi (1 ksi = 6.895 MN/m^2). Under the specified environmental conditions, the material of this gage has a minimum fracture toughness of 37 ksi $\sqrt{in.}$ (1 ksi $\sqrt{in.}$ = 1.099 $\frac{MN}{m^2}\sqrt{m}$) and a threshold stress intensity of 80 percent of K_{Ic}. The plot of flaw-growth rate versus K_{Ii}/K_{Ic} for the material is shown in figure B-4 for σ = 105 ksi (1 ksi = 6.895 MN/m^2). The effect of the stress level on the growth rate is indicated by the equation on the plot. Taking this effect into consideration, the curve is arithmetically integrated, according to the method outlined in reference 8, for three stress levels. These integrated plots (flaw depth versus cycles to fracture) are shown in figure B-5. In the calculations, it was assumed that the value of Q is unity (i.e., the flaws are relatively long with respect to their depth).

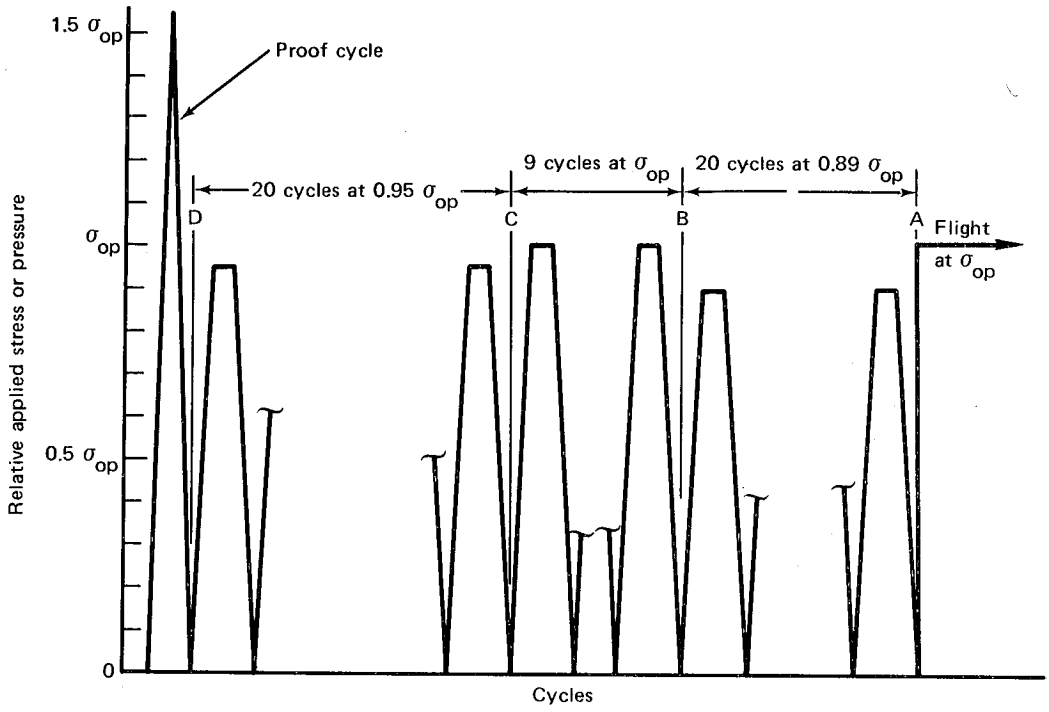

Figure B-3. History of cyclic stresses of a thin-walled vessel.

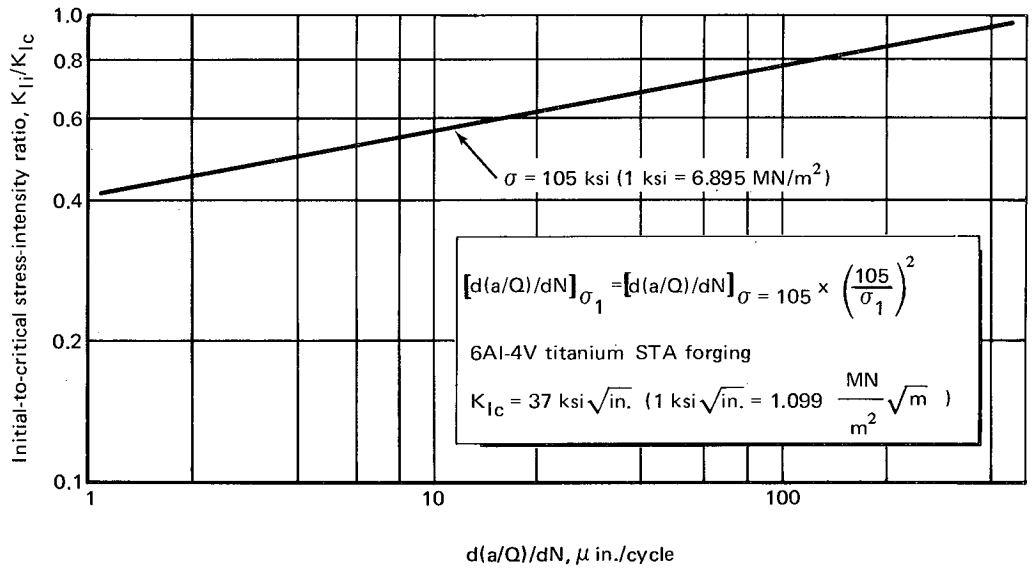

Figure B-4. – Cyclic flaw-growth curve.

Because the threshold stress intensity is 0.80 K_{Ic}, the allowable value of K_{Ii}/K_{Ic} at the beginning of the long-duration flight cycle is 0.80. This requirement is illustrated by point A on the curve of σ_{op} in figure B-5.

The tank-wall stress increases by 11 percent at the end of 20 loading cycles with the maximum stress = 0.89 σ_{op}; however, the flaw size remains the same during the stress increase. This is shown by point A on the plot of 0.89 σ_{op} in figure B-5.

The 20 loading cycles with the maximum stress = 0.89 σ_{op} changes the flaw depth (a) from point A to point B on the plot of 0.89 σ_{op} in figure B-5. Point B is 20 cycles to the right of point A with the cycles being measured along the abscissa of the plot.

The stress decreases by 11 percent at the end of 9 cycles with the maximum stress = σ_{op}. This is shown by point B on the plot of σ_{op} in figure B-5.

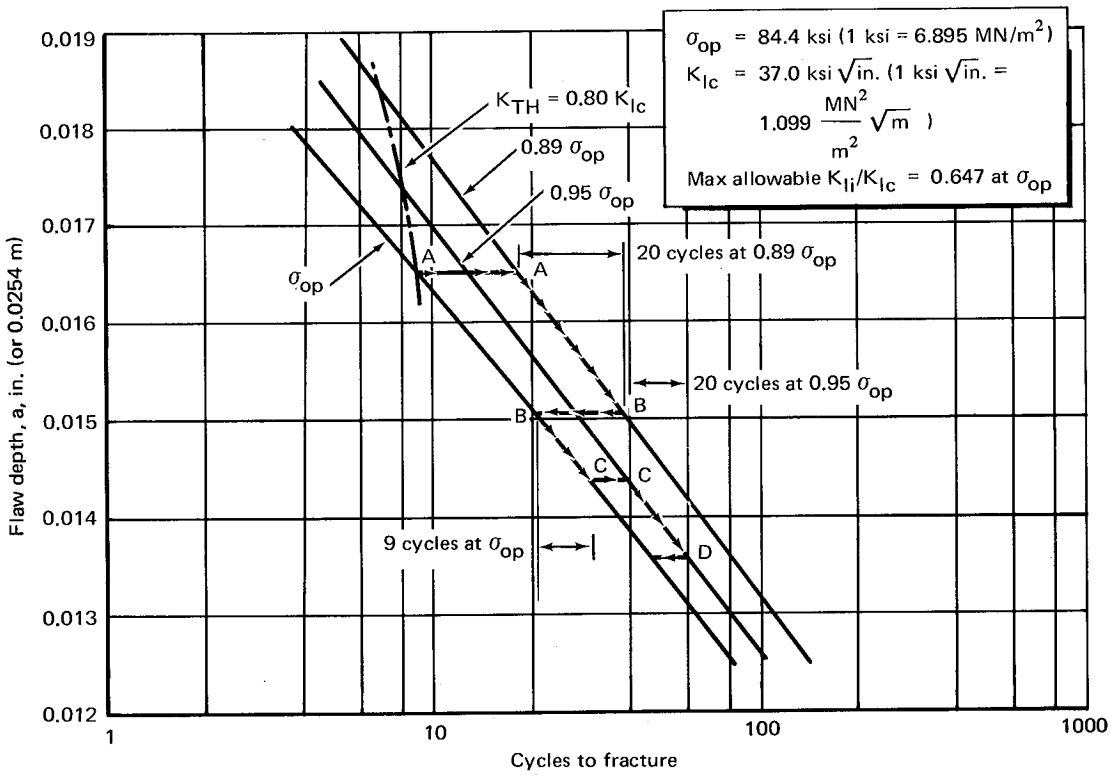

Figure B-5. – Determination of allowable stress-intensity ratio for a thin-walled vessel.

The 9 loading cycles with the maximum stress = σ_{op} changes flaw depth (a) from point B to point C on the plot of σ_{op}. Point C is 9 cycles to the right of point B.

The tank-wall stress increases by 5 percent at the end of 20 loading cycles with the maximum stress = 0.95 σ_{op}. This is shown by point C on the plot of 0.95 σ_{op} in figure B-5.

The 20 loading cycles at 0.95 σ_{op} changes flaw depth (a) from point C to point D on the plot of 0.95 σ_{op}. Point D is 20 cycles to the right of point C. The value of the flaw depth at point D is 0.01356 in. (1 in. = 0.0254 m).

The maximum allowable value of K_{Ii}/K_{Ic} at the end of the proof-test cycle then is given by

$$\frac{K_{Ii}}{K_{Ic}} = \frac{1.1\, M_K \sqrt{\pi a}\ \sigma_{op}}{37.0} \qquad \text{(B-2)}$$

σ_{op} = 84.4 ksi (1 ksi = 6.895 MN/m^2), a/t = 0.01356/0.022 = 0.615, and M_K from figure 3 is 1.25.

Hence, the maximum allowable K_{Ii}/K_{Ic} ratio is 0.647, and the proof factor is a = 1/0.647 = 1.55.

REFERENCES

1. Wessel, E. T.; Clark, W. G.; and Wilson, W. K.: Engineering Methods for the Design and Selection of Materials Against Fracture. U.S. Army Tank and Automotive Center Report, Contract No. DA-30-069-AMC-602(T), 1966.

2. Tiffany, C. F.; and Masters, J.N.: Applied Fracture Mechanics. Fracture Toughness Testing and its Applications. ASTM Spec. Tech. Publication No. 381, 1965, pp. 249-277.

3. Brown, W. F., Jr.; and Srawley, J. E.: Plane Strain Crack Toughness Testing of High Strength Metallic Materials. ASTM Spec. Tech. Publication No. 410, 1966.

4. Irwin, G. R.: Crack Extension Force for a Part-Through Crack in a Plate. Trans. ASME, J. Appl. Mech., Series E, vol. 29, no. 4, Dec. 1962, pp. 651-654.

5. Kobayashi, A. S.: On the Magnification Factors of Deep Surface Flaws. Structural Development Research Memorandum No. 16, The Boeing Co., Dec. 1965.

6. Smith, F. W.: Stress Intensity Factor for a Semi-Elliptical Flaw. Structural Development Research Memorandum No. 17, The Boeing Co., Aug. 1966.

7. Tiffany, C. F.; Masters, J. N.; and Bixler, W. D.: Flaw Growth of 6Al-4V Titanium in a Freon T.F. Environment. NASA CR-99632, 1969.

8. Tiffany, C. F.; Masters, J. N.; and Pall, F. A.: Some Fracture Considerations in the Design and Analysis of Spacecraft Pressure Vessels. Paper presented at the ASM National Metals Congress (Chicago), Oct. 1966.

9. Anon.: ASTM Recommended Practice for Plane-Strain Fracture Toughness Testing of High Strength Metallic Materials Using a Fatigue Cracked Bend Specimen. ASTM Standards, Part 31, May 1969, pp. 1099-1114.

10. Tiffany, C. F.: Investigation of Preflawed 2219 Aluminum Tanks. Rept. D5-13663, The Boeing Co., Aug. 1966.

11. Hall, L. R.; and Tiffany, C. F.: Fracture and Flaw Growth Investigation for 2014-T6 Aluminum Weldments Used in Saturn II LH_2 Tanks. Rept. D5-15737, The Boeing Co., Nov. 1967.

12. Smith, A. B.: Missile Motor Cases. Metals Engineering Quarterly, vol. 3, no. 4, Nov. 1963, pp. 55-63.

13. Johnson, H. A.; et al.: Large Motor Case Evaluation. Annual Progress Report, Vol. II, USAF Contract AF33(615)-1623, June 1965.

14. Srawley, J. E.; and Esgar, J. B.: Investigation of Hydrotest Failure of Thiokol Chemical Corporation 260-inch Diameter SL-1 Motor Case. NASA TM X-1194, 1966.

15. ASTM Special Committee on Fracture Testing of High-Strength Metallic Materials: Progress in the Measurement of Fracture Toughness and the Application of Fracture Mechanics to Engineering Problems. Materials Research and Standards, vol. 4, no. 3, Mar. 1964, pp. 107-119.

16. Shah, R. C.: Fracture Mechanics Assessment of Apollo Launch Vehicle & Spacecraft Pressure Vessels. Vol. 1. Rept. D2-114248-1, The Boeing Co., Nov. 1968.

17. Shank, M. E.; Spaeth, C. E.; Cook, V. W.; and Coyne, J. E.: Solid Fuel Rocket Chambers for Operation at 240,000 psi and Above. Metal Progress, vol. 76, no. 5, Nov. 1959, pp. 74-81 (part I), and vol. 76, no. 6, Dec. 1959, pp. 84-92 (part II).

18. Tiffany, C. F.; and Lorenz, P. M.: An Investigation of Low-Cycle Fatigue Failures Using Applied Fracture Mechanics. Rept. ML-TDR-64-53, Battelle Memorial Institute, May 1964.

19. Tiffany, C. F.; Lorenz, P. M.; and Hall, L. R.: Investigation of Plane Strain Flaw Growth in Thick-Walled Tanks. NASA CR-54837, 1966.

20. Tiffany, C. F.; Lorenz, P. M.; and Shah, R. C.: Extended Loading of Cryogenic Tanks. NASA CR-72252, 1967.

21. Tiffany, C. F.; and Masters, J. N.: Investigation of the Flaw Growth Characteristics of 6Al-4V Titanium Used in Apollo Spacecraft Pressure Vessels. NASA CR-65586, 1967.

22. Masters, J. N.: Cyclic and Sustained Load Flaw Growth Characteristics of 6Al-4V Titanium. NASA CR-92231, 1968.

23. Hall, L. R.: Plain Strain Cyclic Flaw Growth in 2014-T62 Aluminum and 6Al-4V (ELI) Titanium. NASA CR-72396, 1968.

24. Johnson, H. H.; and Paris, P. C.: Subcritical Flaw Growth. Engineering Fracture Mechanics, vol. 1, no. 1, June 1968, pp. 3-45.

25. Peterson, M. H.; Brown, B. F.; Newbegin, R. L.; and Grover, R. E.: Stress Corrosion Cracking of High Strength Steel and Titanium Alloys in Chloride Solutions at Ambient Temperature. Corrosion, vol. 23, no. 5, May 1969, pp. 142-148.

26. Brown, B. F.: A New Stress Corrosion Cracking Test Procedure for High Strength Alloys. Paper presented at the ASTM Arsenal Meeting at Purdue University (Lafayette, Ind.), June 13-18, 1965.

27. Piper, D. E.; Smith, S. H.; and Carter, R. V.: Corrosion Fatigue and Stress Corrosion Cracking in Aqueous Environments. Metals Engineering Quarterly, vol. 8, Aug. 1968, pp. 50-63.

28. Smith, H. R.; Piper, D. E.; and Downey, F. K.: A Study of Stress Corrosion Cracking by Wedge Force Loading. Engineering Fracture Mechanics, vol. 1, no. 1, June 1968, pp. 123-128.

29. Johnson, H. H.; and Willner, A. M.: Moisture and Stable Crack Growth in a High Strength Steel. Applied Materials Research, vol. 4, no. 1, Jan. 1965, pp. 34-40.

30. Steigerwald, E. A.; and Benjamin, W. D.: Stress Corrosion Cracking Mechanisms in Martinistic High Strength Steels. Third Quarterly Progress Report, Contract AF 33(615)-3651, Air Force Materials Laboratory, 1967.

31. Irwin, C. R.: Moisture Assisted Slow Crack Extension in Glass Plate. Memorandum Report 1678, Naval Research Laboratory, 1966.

32. Koetje, E. L.: Report on Failure of T. E. Actuator. Rept. D2-16676-1, The Boeing Co., July 1965.

33. Tiffany, C. F.; Masters, J. N.; and Regan, R. E.: Large Motor Case Technology Evaluation. Rept. AFML-TR-67-190, Air Force Materials Laboratory, Aug. 1967.

34. Lorenz, P. M.: Fracture Toughness and Sustained Flaw Growth Characteristics of Inconel 718 in the Environment of Pressurized Gaseous Hydrogen. Rept. D2-114404-1, The Boeing Co., Oct. 1968.

35. Beachem, C. D.; and Brown, B. F.: A Comparison of Three Specimens for Evaluating the Susceptibility of High Strength Steel to Stress Corrosion Cracking. Internal Report, U.S. Naval Research Laboratory, 1967.

36. Haese, W. P.: Investigation of Fracture of 6Al-4V Titanium in N_2O_4. Rept. D2-24057-1, The Boeing Co., Dec. 1965.

37. Wei, R. P.: Some Aspects of Environment-Enhanced Fatigue Crack Growth. Paper presented at ASTM Fall Meeting (Atlanta, Ga.), Oct. 3, 1968.

38. Barsom, J. M.: Corrosion-Fatigue Crack Propagation Below K_{ISCC}. Paper presented at the National Symposium on Fracture Mechanics at Lehigh University (Bethlehem, Pa.), Aug. 26, 1969.

39. Masters, J. N.; Haese, W. P.; and Finger, R. W.: Investigation of Deep Flaws in Thin Walled Tanks. NASA CR-72606, 1969.

40. Shah, R. C.; and Kobayashi, A. S.: Stress Intensity Factor for an Elliptical Crack Under Arbitrary Normal Loading. Paper presented at the Second National Symposium on Fracture Mechanics at Lehigh University (Bethlehem, Pa.), June 17-19, 1968.

41. Kobayashi, A. S.; Ziv, M.; and Hall, L. R.: Approximate Stress Intensity Factor for an Embedded Elliptical Crack Near Two Parallel Free Surfaces. Int. J. of Fracture Mechanics, vol. 1, no. 2, June 1965, pp. 81-95.

42. Shah, R. C.; and Kobayashi, A. S.: On the Parabolic Crack in an Elastic Solid. Engr. Fracture Mech., vol. 1, no. 2, Aug. 1968, pp. 309-325.

43. Lorenz, P. M.: Compatibility of Tankage Materials with Liquid Propellants. Rept. AFML-TR-69-99, Air Force Materials Laboratory, May 1969.

SYMBOLS

a	semiminor axis of the ellipse $x^2/c^2 + y^2/a^2 = 1$ or crack depth of the semielliptical surface flaw, in. (1 in. = 0.0254 m)
2c	crack length of the semielliptical surface flaw, in.
K_I	plane-strain stress-intensity factor, ksi $\sqrt{\text{in.}}$ (1 ksi $\sqrt{\text{in.}}$ = 1.099 $\frac{\text{MN}}{\text{m}^2}\sqrt{\text{m}}$)
K_{Ic}	plane-strain critical stress-intensity factor or fracture toughness of the material, ksi $\sqrt{\text{in.}}$
K_{Ii}	plane-strain stress-intensity factor at initial conditions, ksi $\sqrt{\text{in.}}$
K_{TH}	plane-strain threshold stress-intensity level, ksi $\sqrt{\text{in.}}$
M_K	stress-intensity magnification factor for deep surface flaws based on Kobayashi's solution
N	number of cycles
Q	flaw-shape parameter = $\phi^2 - 0.212\,(\sigma/\sigma_{ys})^2$
R	ratio of minimum to maximum stress during a cycle
T	time, hr
t	thickness of plate (specimen), in.
α	proof-test factor
θ	angle of integration
σ	uniform gross stress applied at infinity and perpendicular to plane of crack, ksi (1 ksi = 6.895 MN/m^2)
σ_{op}	maximum design operating stress, ksi
σ_{ult}	ultimate strength of the material, ksi
σ_{ys}	uniaxial tensile yield strength of the material, ksi
ϕ	complete elliptical integral of the second kind having modulus k defined as $k = (1 - a^2/c^2)^{\frac{1}{2}}$

SUBSCRIPTS

cr	at critical conditions
i	at initial condition
op	operational

NASA SPACE VEHICLE DESIGN CRITERIA MONOGRAPHS ISSUED TO DATE

SP-8001	(Structures)	Buffeting During Launch and Exit, May 1964
SP-8002	(Structures)	Flight-Loads Measurements During Launch and Exit, December 1964
SP-8003	(Structures)	Flutter, Buzz, and Divergence, July 1964
SP-8004	(Structures)	Panel Flutter, May 1965
SP-8005	(Environment)	Solar Electromagnetic Radiation, June 1965
SP-8006	(Structures)	Local Steady Aerodynamic Loads During Launch and Exit, May 1965
SP-8007	(Structures)	Buckling of Thin-Walled Circular Cylinders, September 1965 Revised August 1968
SP-8008	(Structures)	Prelaunch Ground Wind Loads, November 1965
SP-8009	(Structures)	Propellant Slosh Loads, August 1968
SP-8010	(Environment)	Models of Mars Atmosphere (1967), May 1968
SP-8011	(Environment)	Models of Venus Atmosphere (1968), December 1968
SP-8012	(Structures)	Natural Vibration Modal Analysis, September 1968
SP-8013	(Environment)	Meteoroid Environment Model – 1969 [Near Earth to Lunar Surface], March 1969
SP-8014	(Structures)	Entry Thermal Protection, August 1968
SP-8015	(Guidance and Control)	Guidance and Navigation for Entry Vehicles, November 1968
SP-8016	(Guidance and Control)	Effects of Structural Flexibility on Spacecraft Control Systems, April 1969
SP-8017	(Environment)	Magnetic Fields – Earth and Extraterrestrial, March 1969
SP-8018	(Guidance and Control)	Spacecraft Magnetic Torques, March 1969
SP-8019	(Structures)	Buckling of Thin-Walled Truncated Cones, September 1968
SP-8020	(Environment)	Mars Surface Models [1968], May 1969
SP-8021	(Environment)	Models of Earth's Atmosphere (120 to 1000 km), May 1969
SP-8023	(Environment)	Lunar Surface Models, May 1969
SP-8024	(Guidance and Control)	Spacecraft Gravitational Torques, May 1969
SP-8025	(Chemical Propulsion)	Solid Rocket Motor Metal Cases, April 1970

SP-8026	(Guidance and Control)	Spacecraft Star Trackers, July 1970
SP-8027	(Guidance and Control)	Spacecraft Radiation Torques, October 1969
SP-8028	(Guidance and Control)	Entry Vehicle Control, November 1969
SP-8029	(Structures)	Aerodynamic and Rocket-Exhaust Heating During Launch and Ascent, May 1969
SP-8031	(Structures)	Slosh Suppression, May 1969
SP-8032	(Structures)	Buckling of Thin-Walled Doubly Curved Shells, August 1969
SP-8033	(Guidance and Control)	Spacecraft Earth Horizon Sensors, December 1969
SP-8034	(Guidance and Control)	Spacecraft Mass Expulsion Torques, December 1969
SP-8035	(Structures)	Wind Loads During Ascent, June 1970
SP-8036	(Guidance and Control)	Effects of Structural Flexibility on Launch Vehicle Control Systems, February 1970
SP-8046	(Structures)	Landing Impact Attenuation for Nonsurface-Planing Landers, April 1970

NASA-Langley, 1970 —— 32